iScience

CellPress
OPEN ACCESS

Article

IL-15 boosts activated HBV core-specific CD8$^+$ progenitor cells via metabolic rebalancing in persistent HBV infection

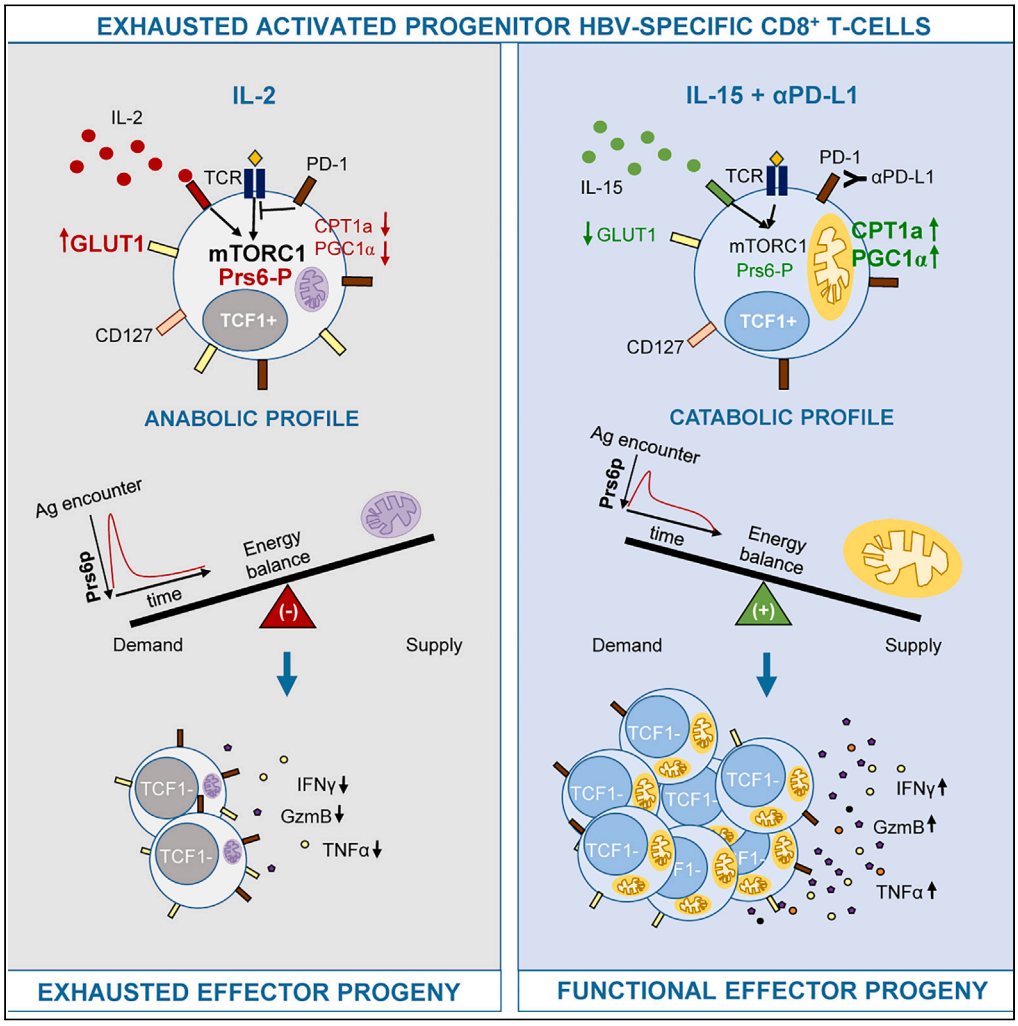

Julia Peña-Asensio, Henar Calvo-Sánchez, Joaquín Miquel, Eduardo Sanz-de-Villalobos, Alejandro González-Praetorius, Miguel Torralba, Juan-Ramón Larrubia

juan.larrubia@uah.es

Highlights

IL-15 improves functionality of exhausted HBV core-specific progenitor CD8$^+$ T-cells

By improving the balance between energy demand and supply

Thru decreasing T cell stimulation intensity and enhancing catabolic metabolism

IL-15 effects plus PD-1 blockade restores functionality of deeply exhausted progeny

Peña-Asensio et al., iScience 27, 108666
January 19, 2024
https://doi.org/10.1016/j.isci.2023.108666

iScience

CellPress
OPEN ACCESS

Article

IL-15 boosts activated HBV core-specific CD8$^+$ progenitor cells via metabolic rebalancing in persistent HBV infection

Julia Peña-Asensio,[1,6] Henar Calvo-Sánchez,[2,5,6] Joaquín Miquel,[2,6] Eduardo Sanz-de-Villalobos,[2,6] Alejandro González-Praetorius,[3,6] Miguel Torralba,[4,5,6] and Juan-Ramón Larrubia[2,5,6,7,*]

SUMMARY

A rebalance between energy supply and demand in HBV-specific-CD8$^+$ activated progenitor (AP) cells could restore the functionality of proliferative progeny (PP) in e-antigen(Ag)-negative chronic hepatitis B (CHBe(−)). We observed that quiescent progenitor (QP [TCF1$^+$/FSC^{low}]) HBVcore-specific-CD8$^+$ cells displayed a memory-like phenotype. Following Ag-encounter, the generated AP [TCF1$^+$/FSC^{high}] subset maintained the PD1$^+$/CD127$^+$ phenotype and gave rise to proliferative progeny (PP [TCF1$^-$/FSC^{high}]). In AP cells, IL-15 compared to IL2 decreased the initial mTORC1 boost, but maintained its activation longer linked to a catabolic profile that correlated with enhanced PP effector abilities. In nucleos(t)ide analogue (NUC)-treated CHBe(−), AP subset showed an anabolic phenotype associated with a dysfunctional PP pool. In CHBe(−) cases with low probability of HBVcore-specific-CD8$^+$ cell on-NUC-treatment restoration, according to a clinical predictive model, IL-15/anti-PD-L1 treatment re-established their reactivity. Therefore, IL-15 could improve AP pool energy balance by decreasing intensity but extending T cell activation and by inducing a more catabolic metabolism.

INTRODUCTION

An effective hepatitis B virus (HBV)-specific CD8$^+$ T cell response is essential to keep HBV under control but unfortunately these cells become exhausted during persistent HBV infection.[1] Exhausted virus-specific CD8$^+$ T-cells comprise the progenitor and progeny cell pools. The former is responsible for maintaining a dysfunctional effector subset capable of keeping viral replication in check during chronic infection.[2] These progenitor cells carry out asymmetric cell division (ACD) and self-renewal and are characterized by the expression of the transcription factor T cell factor(TCF)-1[3–6] and can be found in central and peripheral compartments.[7] After antigen (Ag) encounter, this quiescent precursor (QP) subset follows a linear differentiation,[7] starting with transformation into the activated progenitor (AP) cell pool, which develops a more intense metabolism to give rise to the effector proliferative progeny (PP), but still maintains ACD ability and are capable of reacquiring a more quiescent phenotype.[7–9]

Mitochondrial metabolism is a key factor for the AP cell pool to carry-out its functions. Despite their activation, these cells need to preserve catabolic features defined by oxidative phosphorylation (OXPHOS), fatty acid oxidation (FAO), and low generation of reactive oxygen species.[9,10] This process involves the phosphoinositide 3-kinase (PI3K) pathway.[11] T cell receptor (TCR) triggering induces PI3K/protein kinase B (Akt)/mammalian target of rapamycin (mTOR)C1 activation, leading the progeny to an anabolic state. Nevertheless, mTORC1 activation is also necessary to promote catabolic reprogramming and memory T cell generation in the progenitor cell pool.[4] A balance between the intensity of T cell activation and the ability to meet the energy needs in the AP cell subset could determine the functionality of the PP.

During persistent viral infections, the progenitor cell subset displays an exhausted phenotype defined by programmed cell death protein-1 (PD-1^{dim}) expression but remains capable of responding to immunotherapy strategies.[2,12–14] PD-1 receptor counteracts co-stimulatory signals that are essential for complete T cell activation.[15] Monotherapy strategies blocking PD-1/PD-ligand(L)1 pathway can restore T cell function in some cases, but fails in others with a more intense exhaustion level.[16] PD-1, by restraining Ag-dependent TCR signals, protects exhausted progenitor cells.[17] Blockade of inhibitory checkpoints in these cells may not be sufficient to achieve T cell restoration due to the coexisting impairment of energy production, being unable these cells to meet the necessary extra-energy demands after full stimulation.

[1]Department of Biology of Systems, University of Alcalá, 28801 Alcalá de Henares, Madrid, Spain
[2]Section of Gastroenterology, Guadalajara University Hospital, 19002 Guadalajara, Castilla La-Mancha, Spain
[3]Section of Microbiology, Guadalajara University Hospital, 19002 Guadalajara, Castilla La-Mancha, Spain
[4]Service of Internal Medicine, Guadalajara University Hospital, 19002 Guadalajara, Castilla La-Mancha, Spain
[5]Department of Medicine & Medical Specialties, University of Alcalá, 28801 Alcalá de Henares, Madrid, Spain
[6]Instituto de Investigación Sanitaria de Castilla La-Mancha (IDISCAM), 45071 Toledo, Castilla La-Mancha, Spain
[7]Lead contact
*Correspondence: juan.larrubia@uah.es
https://doi.org/10.1016/j.isci.2023.108666

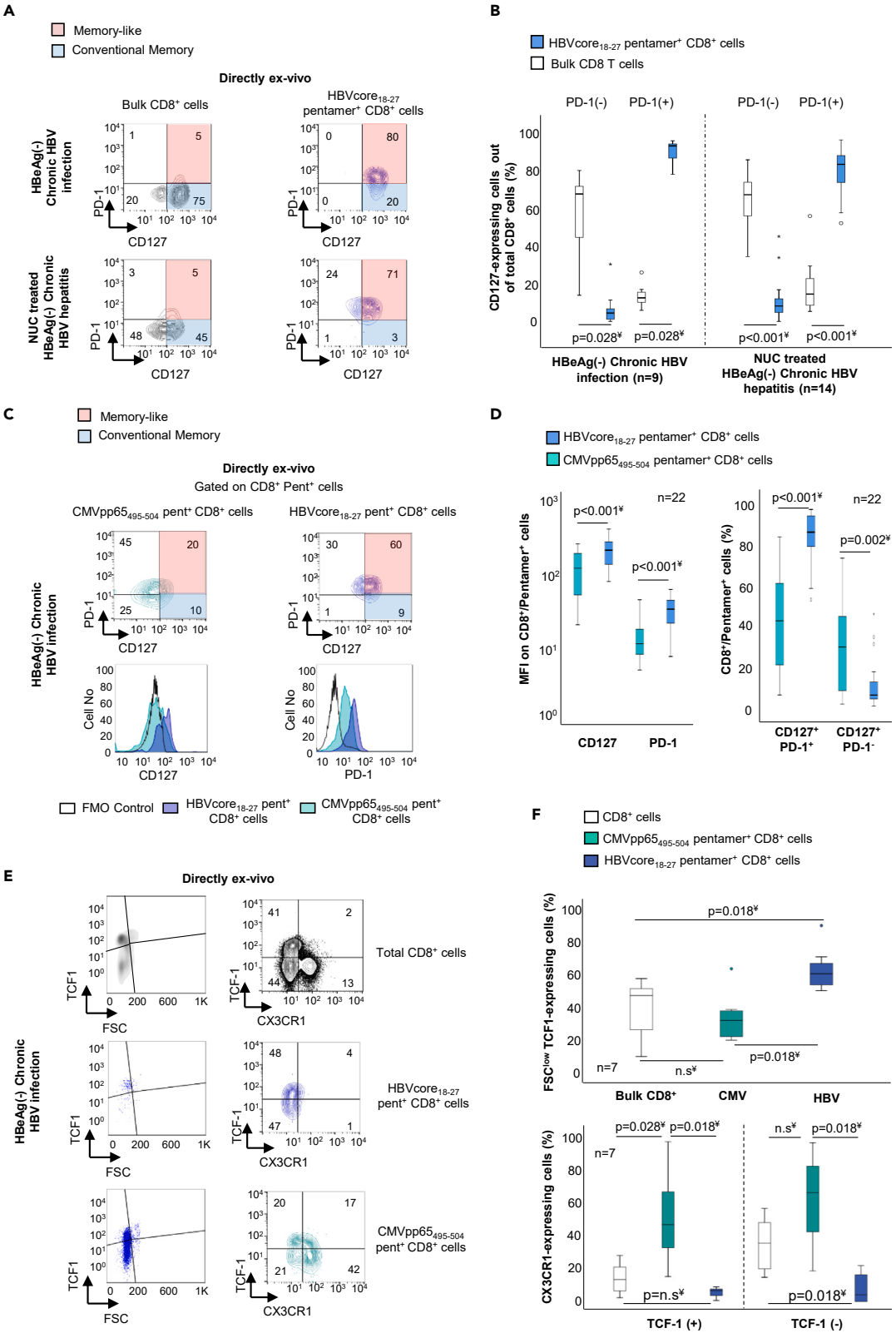
A
Memory-like
Conventional Memory
Directly ex-vivo
Bulk CD8⁺ cells
HBVcore18-27 pentamer⁺ CD8⁺ cells
HBeAg(-) Chronic HBV infection
NUC treated HBeAg(-) Chronic HBV hepatitis
PD-1
CD127
B
HBVcore18-27 pentamer⁺ CD8⁺ cells
Bulk CD8 T cells
PD-1(-)
PD-1(+)
CD127-expressing cells out of total CD8⁺ cells (%)
p=0.028¥
p=0.028¥
p<0.001¥
p<0.001¥
HBeAg(-) Chronic HBV infection (n=9)
NUC treated HBeAg(-) Chronic HBV hepatitis (n=14)
C
Memory-like
Conventional Memory
Directly ex-vivo
Gated on CD8⁺ Pent⁺ cells
CMVpp65495-504 pent⁺ CD8⁺ cells
HBVcore18-27 pent⁺ CD8⁺ cells
HBeAg(-) Chronic HBV infection
Cell No
FMO Control
HBVcore18-27 pent⁺ CD8⁺ cells
CMVpp65495-504 pent⁺ CD8⁺ cells
D
HBVcore18-27 pentamer⁺ CD8⁺ cells
CMVpp65495-504 pentamer⁺ CD8⁺ cells
MFI on CD8⁺/Pentamer⁺ cells
p<0.001¥
p<0.001¥
n=22
CD127
PD-1
CD8⁺/Pentamer⁺ cells (%)
p<0.001¥
p=0.002¥
n=22
CD127⁺ PD-1⁺
CD127⁺ PD-1⁻
E
Directly ex-vivo
HBeAg(-) Chronic HBV infection
TCF1
FSC
TCF-1
CX3CR1
Total CD8⁺ cells
HBVcore18-27 pent⁺ CD8⁺ cells
CMVpp65495-504 pent⁺ CD8⁺ cells
F
CD8⁺ cells
CMVpp65495-504 pentamer⁺ CD8⁺ cells
HBVcore18-27 pentamer⁺ CD8⁺ cells
FSClow TCF1-expressing cells (%)
p=0.018¥
p=0.018¥
n=7
n.s¥
Bulk CD8⁺
CMV
HBV
CX3CR1-expressing cells (%)
p=0.028¥
p=0.018¥
n.s¥
p=0.018¥
n=7
p=n.s¥
p=0.018¥
TCF-1 (+)
TCF-1 (-)

Figure 1. Directly *ex vivo* peripheral HBV-specific CD8$^+$ "memory-like" progenitor cell pool

(A) BD FACS Calibur contour-plots depicting the co-expression of PD-1 and CD127 molecules on peripheral total and HBVcore$_{18\text{-}27}$-specific CD8$^+$ cells in eAg(−) chronic HBV infection (CIBe(−)) and nucleos(t)ide analogue (NUC)-treated chronic hepatitis B (CHBe(−)).

(B) Boxplots summarizing the percentage of CD127$^+$ PD-1-expressing and PD-1$^-$ cells out of total CD8$^+$ and HBVcore$_{18\text{-}27}$-specific CD8$^+$ cells in CIBe(−) and NUC-treated CHBe(−).

(C) Representative BD FACS Caliburcontour-plots and histograms describing the level of PD-1 and CD127 expression and the percentage of conventional memory and memory-like peripheral Ag-specific CD8$^+$ cells in paired HBV and CMV infections in a CIBe(−) patient.

(D) Boxplots summarizing the expression level of PD-1 and CD127 and the frequency of CD127$^+$ PD-1$^+$ and PD-1$^-$ cells on peripheral HBV and CMV-specific CD8$^+$ cell populations in CIBe(−).

(E) BD FACS Caliburdensity-, contour- and dot-plots showing the TCF1 and CX3CR1 expression in peripheral total and HBV and CMV-specific CD8$^+$ cells from a CIBe(−) patient.

(F) Boxplots summarizing the percentage of FSC^{low} TCF1-expressing and the CXCR3-expressing TCF1 positive and negative cells in peripheral total and Ag-specific CD8$^+$ cells in CIBe(−). CMV: cytomegalovirus, FMO: fluorescence minus one, FSC: forward scatter, HBV: hepatitis B virus, MFI: mean fluorescence intensity, NUC: nucleos(t)ide analogue, Pent: pentamer. ¥Wilconxon test. Data are represented as median plus interquartile range.

Interleukin (IL)-15 is a pleotropic cytokine involved in T cell survival, proliferation and memory formation.[18–23] Repeated doses of this cytokine can induce cell exhaustion by intense mTORC1 activation through continuous gamma chain-receptor triggering.[24] However, T cell stimulation in an IL-15-rich environment can modulate mTORC1 activity and favor FAO and memory generation,[25] which could make this strategy useful for improving AP cell functionality.

Natural history of chronic HBV infection has several distinctive phases defined by the interplay between immune response and HBV replication.[26] During e-Ag negative chronic HBV infection (CIBe(−)) phase, formerly called "inactive carrier", the immune system is able to keep HBV closely controlled. This phase is characterized by normal transaminases and low HBV DNA level. Nevertheless, during eAg(−) chronic hepatitis B (CHBe(−)) stage, the immune response is exhausted, leading to high level of HBV replication and liver inflammation.[1,27] In those cases, where the peripheral AP pool is expected to be little exhausted, as in CIBe(−), IL-15 treatment might be sufficient to enhance its functionality. In contrast, in more exhausted cases, as in CHBe(−) treated for a short period of time with nucleos(t)ide analogues (NUC),[28] the combination of IL-15 with other immunomodulatory therapies, such as PD-1/PD-L1 blockade, might be necessary, as both strategies could have a positive effect on mitochondrial metabolism and TCR triggering.[29–32]

Previous work has shown that early-onset, long-term treatment with NUC can restore HBV-specific cytotoxic T cell response in CHBe(−) cases with short-duration infection, which is associated with functional cure after treatment discontinuation.[28] Nevertheless, about 2/3 of CHBe(−) cases do not develop functional cure after treatment stop.[33,34] In these cases, realignment between energy demands and supply in the AP pool should be explored as strategy to achieve functional cure. In this work, we demonstrate that IL-15 *in vitro* treatment induces both an intermediate but sustained mTORC1 activation and a catabolic profile in the AP subset, resulting in an enhanced effector capacity in HBV-specific CD8$^+$ T cell progeny. Furthermore, this effect of IL-15 can be harnessed in combination with anti-PD-L1 to restore HBV-specific CD8$^+$ T cell reactivity in CHBe(−) patients with low likelihood of developing a functional response during NUC treatment.[28]

RESULTS

Peripheral HBV-specific CD8$^+$ cell pool is enriched in quiescent progenitor cells displaying a memory-like phenotype during chronic HBV infection

We carried out a directly *ex vivo* analysis of the peripheral pool of HBVcore$_{18\text{-}27}$-specific CD8$^+$ cells expressing the memory marker CD127 in patients with CIBe(−) and NUC-treated CHBe(−). We observed that 96% (interquartile range (IQR) 7%) and 92% (IQR 15%) of the peripheral pool of quiescent cells in CIBe(−) and CHBe(−) expressed CD127 respectively. We searched for the "memory-like" phenotype, characterized by CD127 expression but also by the presence of the exhaustion/activation marker PD-1.[12] We observed this phenotype in 93% (IQR 10%) and 83% (IQR 17%) of peripheral CD8$^+$/pentamer$^+$ cells in CIBe(−) and CHBe(−) respectively, while the bulk of the CD8$^+$ CD127$^+$ population was PD-1 negative, as corresponds to the conventional memory pool. (Figures 1A and 1B).

We also compared the frequency of peripheral HBVcore$_{18\text{-}27}$- and cytomegalovirus (CMV)pp65$_{495\text{-}04}$-specific CD8$^+$ "memory-like" cells in paired samples of CIBe(−). We observed a higher PD-1 and CD127 expression in HBV-specific than in CMV-specific cells, resulting in a "memory-like" enrichment in the HBV-specific pool of approximately 2-fold the level observed in the CMV population and, a higher frequency of conventional memory cells in the CMV subset (Figures 1C and 1D).

We analyzed whether the memory-like CD127$^+$/PD-1$^+$-expressing HBV-specific CD8$^+$ peripheral pool could correspond to the peripheral memory subset described by Gerlach et al.[35] by testing the level of CX3CR1^{int} expression in TCF1$^+$ cells from CIBe(−). We detected an enrichment of QP cells (TCF1$^+$ FSC^{low}) in the HBV-specific CD8$^+$ cells, approximately twice the frequency observed in the CMV-specific pool. No TCF1-expressing HBVcore$_{18\text{-}27}$-Pentamer$^+$ CD8$^+$ cell expressed CX3CR1, whereas we observed CX3CR1^{int} expression in 46% (IQR 58%) of TCF1$^+$ cells in the CMV-specific CD8$^+$ cell pool (Figures 1E and 1F).

IL-15 favors a weaker but longer-lasting activation of peripheral HBV-specific CD8$^+$ activated progenitor cells after Ag encounter

To understand the differentiation process of quiescent peripheral memory-like HBV-specific CD8$^+$ cells after Ag-encounter in persistent HBV infection, we checked the *in vitro* dynamics of progenitor and progeny cell pools after Ag-specific TCR triggering in four CIBe(−) patients and

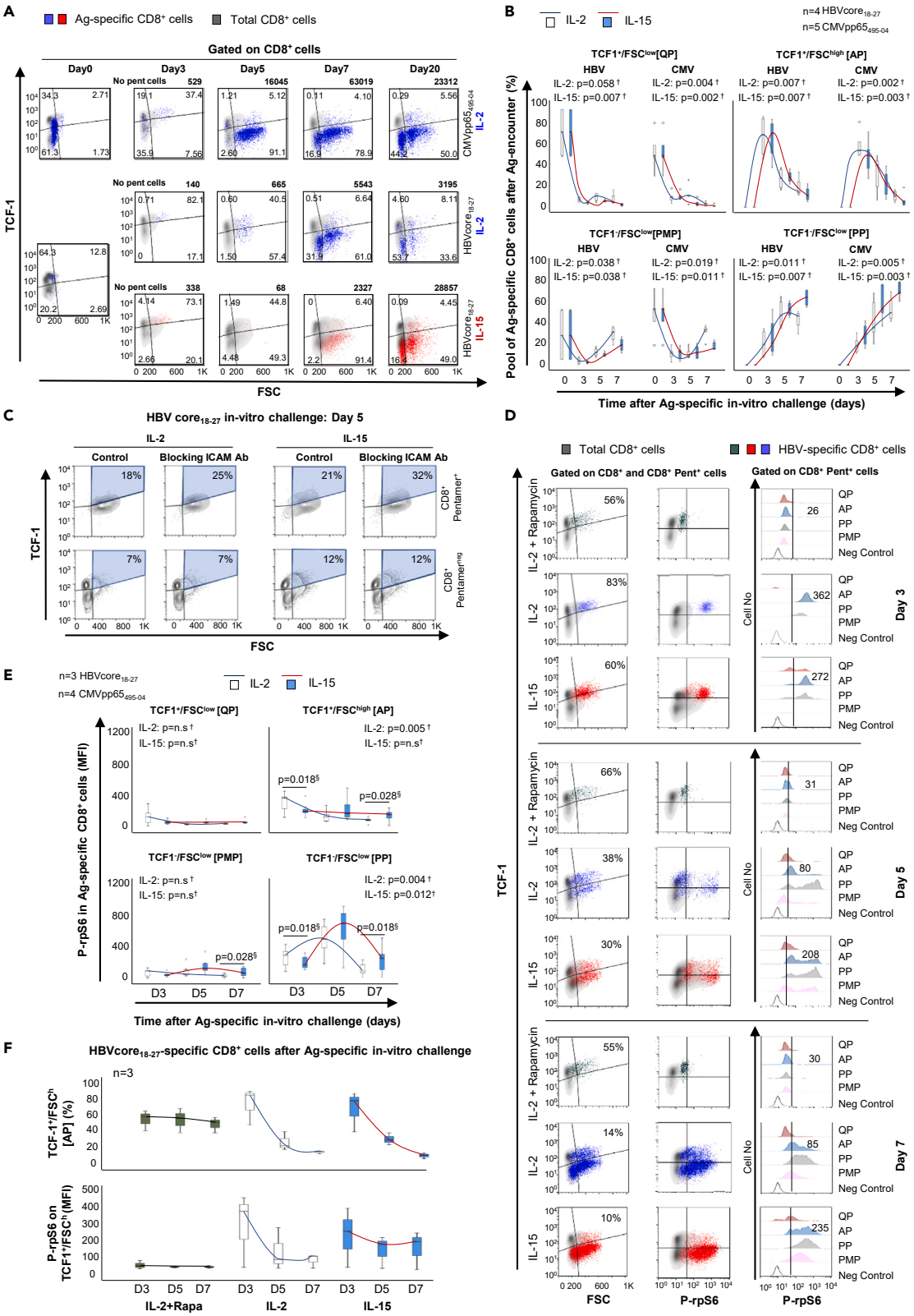
A
Ag-specific CD8+ cells
Total CD8+ cells
Gated on CD8+ cells
Day0
Day3
Day5
Day7
Day20
TCF-1
FSC
CMVpp65495-04 IL-2
HBVcore18-27 IL-2
HBVcore18-27 IL-15
B
IL-2
IL-15
n=4 HBVcore18-27
n=5 CMVpp65495-04
TCF1+/FSClow[QP]
TCF1+/FSChigh [AP]
TCF1-/FSClow[PMP]
TCF1-/FSClow [PP]
HBV
CMV
Pool of Ag-specific CD8+ cells after Ag-encounter (%)
Time after Ag-specific in-vitro challenge (days)
C
HBV core18-27 in-vitro challenge: Day 5
IL-2
IL-15
Control
Blocking ICAM Ab
CD8+ Pentamer+
CD8+ Pentamer-neg
TCF-1
FSC
D
Total CD8+ cells
HBV-specific CD8+ cells
Gated on CD8+ and CD8+ Pent+ cells
Gated on CD8+ Pent+ cells
IL-2 + Rapamycin
IL-2
IL-15
Cell No
Day 3
Day 5
Day 7
QP
AP
PP
PMP
Neg Control
FSC
P-rpS6
E
n=3 HBVcore18-27
n=4 CMVpp65495-04
P-rpS6 in Ag-specific CD8+ cells (MFI)
Time after Ag-specific in-vitro challenge (days)
F
HBVcore18-27-specific CD8+ cells after Ag-specific in-vitro challenge
n=3
TCF-1+/FSCh [AP] (%)
P-rpS6 on TCF1+/FSCh (MFI)
IL-2+Rapa
IL-2
IL-15

Figure 2. Characterization of the peripheral pool of activated Ag-specific CD8$^+$ progenitor cells

(A) BD FACS Calibur dot-plots showing the dynamics of Ag-specific CD8$^+$ cells after specific *in vitro* challenge in presence of IL-2 or IL-15, according to TCF1 expression and FSC level. CD8$^+$ cell pools defined by the FSC and TCF1 level: FSC^{low} comprises quiescent progenitor (TCF1$^+$; QP) and post-mitotic progeny (TCF1$^-$; PMP) cells and FSC^{high} encompasses activated progenitor cells (TCF1$^+$; AP) and effector proliferative progeny (TCF1$^-$; PP). On the background, gray density plots show the total CD8$^+$ cell subset distribution as control. In the foreground, red and blue dot-plots represent the Ag-specific CD8$^+$ cells stimulated in presence of IL-2 (blue) or IL-15 (red). The figures in each dot-plot quadrant show the percentage of CD8$^+$/Pentamer$^+$ cells out of total Ag-specific CD8$^+$ cells. The figure in the upper-right corner describes the total number of CD8$^+$/Pentamer$^+$ cells acquired per million of seeded peripheral blood mononuclear cells.

(B) Boxplots summarizing the dynamics of each Ag-specific CD8$^+$ cell progenitor and progeny subset after Ag encounter, according to FSC level and TCF1 expression, during one-week follow-up.

(C) Illustrative BD FACS Calibur contour-plot showing the frequency of HBVcore$_{18\text{-}27}$-specific CD8$^+$ cells in the activated progenitor pool after 5-day Ag-specific *in vitro* challenge in presence and absence of ICAM-I blocking mAb.

(D) BD FACS Calibur dot-plots and histograms showing the dynamic of phosphorylated ribosomal protein S6 (P-rpS6) in the different HBVcore$_{18\text{-}27}$-specific CD8$^+$ cell pools after Ag-encounter in presence of IL-2 or IL-15 or IL-2 plus rapamycin. Background gray density plots show the total CD8$^+$ cells as control. The figure in the upper-right quadrant in each dot-plot represents the frequency of AP cells out of total HBV-specific CD8$^+$ cells. The figure in each histogram plot shows the P-rpS6 MFI in the AP pool.

(E) Boxplots depicting the P-rpS6 MFI dynamics on the different Ag-specific CD8$^+$ cell pools after Ag encounter.

(F) Boxplots summarizing the frequency of AP (TCF1$^+$/FSC^{high}) cells and the P-rpS6 level in this pool of HBV-core$_{18\text{-}27}$ specific CD8$^+$ cells at days: 3, 5 and 7 of culture in presence of rapamycin plus IL2 or IL-2 or IL-15 treatment. Ab: antibody, AP: activated progenitor, CMV: cytomegalovirus, D: day, FSC: forward scatter, HBV: hepatitis B virus, MFI: mean fluorescence intensity, Neg: negative, pent: CD8$^+$/Pentamer$^+$ cells, PMP: post-mitotic progeny, PP: proliferative progeny, QP: quiescent progenitor. †Friedman test. §Wilconxon test. Data are represented as median plus interquartile range.

five CMV infection cases in presence of IL-2 or IL-15. We defined four different CD8$^+$ progenitor and progeny cell subsets according to TCF-1 expression and forward scatter (FSC) level on flow cytometry analysis. The QP cell pool (TCF-1$^+$/FSC^{low}), disappeared after Ag encounter. The AP subset frequency (TCF-1$^+$ FSC^{high}), peaked at day 3 of culture with IL2 and IL-15 and progressively decreased thereafter. In IL-2 cultures, PP subset (TCF-1$^-$ FSC^{high}), progressively increased until day-5, to enter the contraction phase on day-7. Nevertheless, HBV- and CMV-specific proliferative progenies treated with IL-15 experienced an inflationary state on day-7 compared to IL-2 treatment ($p = 0.008$, Wilcoxon test). Finally, in IL-2 group, the post-mitotic proliferative (PMP) cell pool (TCF-1$^-$ FSC^{low}), was small on day-3 and day-5, with a subsequent increase on day-7, whereas this pool remained low in IL-15 cultures ($p = 0.008$, Wilcoxon test), (Figures 2A and 2B).

To analyze the involvement of asymmetric cell division (ACD) in the role of the AP cell pool in giving rise to progeny, we impaired this function by blocking the interaction of intercellular adhesion molecule 1 (ICAM-I) with its ligand, lymphocyte function-associated antigen 1 (LFA-1), in HBV-core$_{18\text{-}27}$-specific CD8$^+$ cells from one patient with CIBe(−). In addition to the TCR/human leukocyte antigen (HLA)-I interaction, ICAM-I/LFA-1 is required at the immune synapse to promote ACD.[4] In both IL-2 and IL-15 cultures, ICAM-I blocking antibodies increased the frequency of TCF1$^+$ FSC^{high} cells after 5-day Ag-specific *in vitro* challenge, suggesting the presence of more self-renewal and less ACD than without blocking ICAM-I/LFA-1 interaction (Figure 2C).

After TCR activation, an initial mTORC1 down-modulation is necessary to promote ACD, but after this initial 24-36h suppression, partial activation of mTORC1 is required to maintain ACD.[4] We longitudinally assessed the expression of phosphorylated ribosomal protein S6 (P-rpS6) as a readout of mTORC1 activation. We observed a peak of P-rpS6 expression at day-3 of culture in the IL-2-treated AP cell pool with a subsequent decline, whereas IL-15-treated AP cells showed a lower initial increase of P-rpS6, but maintained the same moderate level throughout culture, which meant a significantly higher mTORC1 activation at day-7 with IL15 than with IL-2. Similar but delayed dynamics were observed in PP cell subset with IL-2, peaking P-rpS6 on day 5 with a subsequent decrease on day 7. Once again, IL-15 treatment maintained a higher level of P-rpS6 on day 7 in PP cells, which could be related to the inflation process observed in the IL-15 treated PP pool (Figures 2D and 2E).

To better understand the requirement for mTORC1 activation to carry-out the ACD in the AP pool, after 24h of Ag-specific *in vitro* challenge, we added rapamycin to the culture. In the HBVcore$_{18\text{-}27}$-specific cultures treated with rapamycin plus IL-2, we observed a correlation between the absence of P-rpS6 expression and an enrichment in the frequency of AP cells at day-5 and 7 compared to those receiving only IL-2 or IL-15, which could suggest more self-renewal and less ACD in the AP subset after blocking mTORC1 activity (Figures 2D and 2F).

Activated peripheral HBV-specific CD8$^+$ progenitor cells from HBV inactive carriers (CIBe(−)) show a catabolic phenotype CPT1^{high}, PGC1^{high} linked to high Glut1 expression

We tested T cell lines at day 7, to ensure that AP cells have performed their three initial divisions, before giving rise the PP pool by ACD.[8] On day-7 after Ag-specific *in vitro* challenge, we tested the expression of carnitine palmitoyltransferase (CPT)1a, peroxisome proliferator-activated receptor-gamma coactivator (PGC)-1α and glucose transporter (Glut)1 in all different subsets of HBVcore$_{18\text{-}27}$-specific CD8$^+$ cells from CIBe(−) patients. The TCF1$^+$ FSC^{high} (AP) pool maintained the memory-like phenotype (CD127$^+$ PD1$^+$), with higher CD127 expression than the PP and PMP pools and with PD-1 expression similar to that of the PP subset but higher than that of the PMP pool (Figure 3). AP cells showed mitochondrial biogenesis induction with intense PGC1a expression, higher than that of the PP and PMP subsets (Figure 3). These TCF1$^+$/FSC^{high} cells also exhibited favored OXPHOS, as they expressed higher levels of CPT1a than those of the PP and PMP subsets (Figure 3). Finally, the AP pool had also induced the expression of the glucose transporter Glut1 at the same level as the PP subset and higher than the PMP (Figure 3).

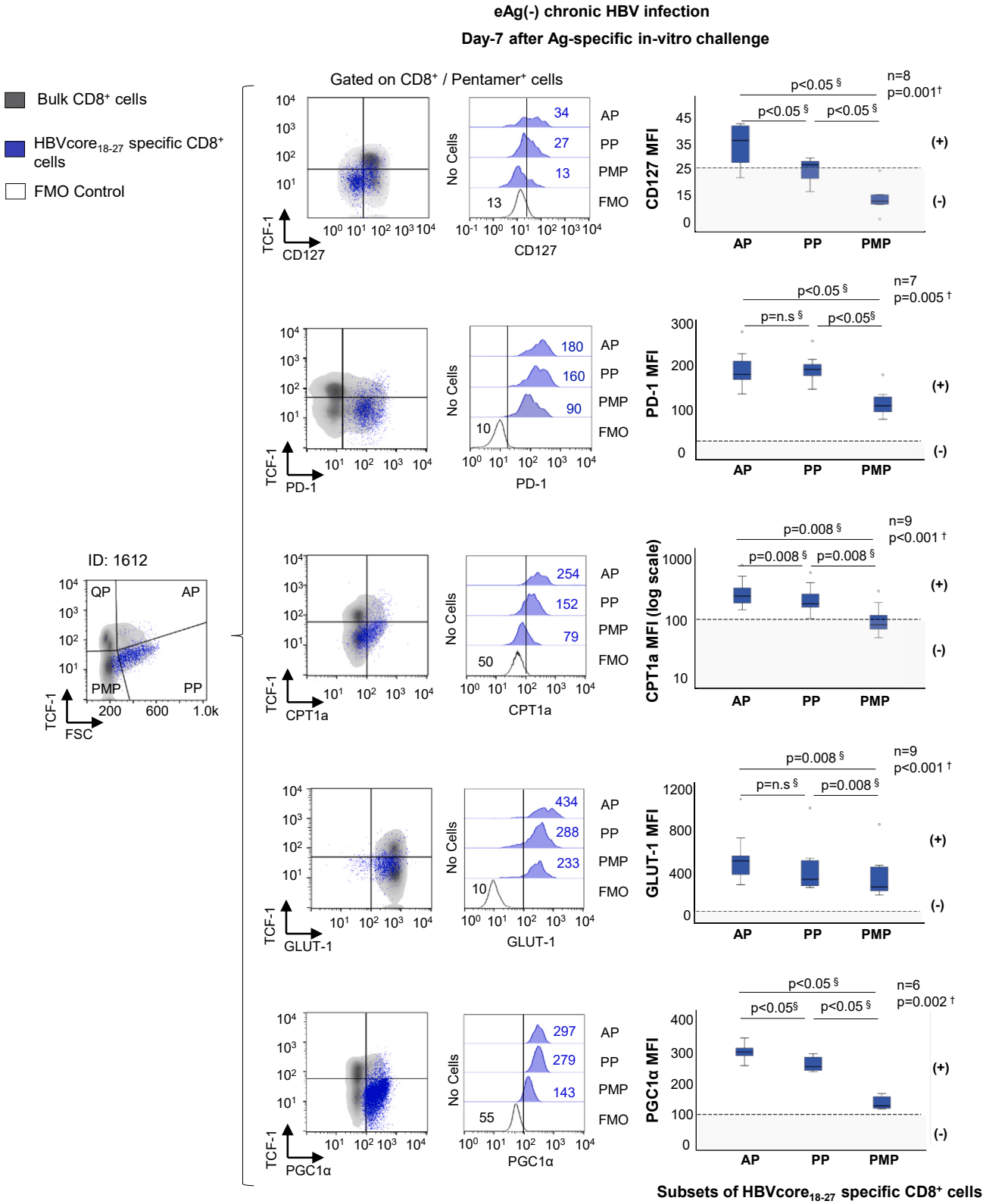
eAg(-) chronic HBV infection
Day-7 after Ag-specific in-vitro challenge
Bulk CD8⁺ cells
HBVcore18-27 specific CD8⁺ cells
FMO Control
ID: 1612
QP
AP
PMP
PP
TCF-1
FSC
Gated on CD8⁺ / Pentamer⁺ cells
CD127
PD-1
CPT1a
GLUT-1
PGC1α
No Cells
AP
PP
PMP
FMO
34
27
13
180
160
90
254
152
79
434
288
233
297
279
143
CD127 MFI
PD-1 MFI
CPT1a MFI (log scale)
GLUT-1 MFI
PGC1α MFI
p<0.05 §
p=0.001†
p=n.s §
p<0.05§
p=0.005 †
p=0.008 §
p<0.001 †
p=0.002 †
(+)
(-)
Subsets of HBVcore18-27 specific CD8⁺ cells

Figure 3. Metabolic profile of the different HBV-specific CD8$^+$ progenitor and progeny pools after Ag-specific *in vitro* challenge

Representative BD FACS Calibur dot-plots and histograms and summarizing box-plots from eAg(−) chronic HBV infection patients (inactive carriers), describing the expression of CD127, PD-1, CPT1a, PGC1α and Glut-1 in HBVcore$_{18\text{-}27}$-specific CD8$^+$ progenitor and progeny cell pools after 7-day Ag-specific *in vitro* challenge. Blue dots in the foreground represent HBV-specific CD8$^+$ cells and gray density plots in the background show the total CD8$^+$ cell distribution as control. The dashed line in the box-plot charts represents the upper-limit of MFI FMO distribution. AP: activated progenitor, FMO: fluorescence minus one, FSC: forward scatter, HBV: hepatitis B virus, ID: patient's identification, MFI: mean fluorescence intensity, PMP: post-mitotic progeny, PP: proliferative progeny, QP: quiescent progenitor. (+) Positive expression, (−) Negative expression. †Friedman test. §Wilconxon test. Data are represented as median plus interquartile range.

IL-15 induced a more catabolic profile in the activated progenitor cell pool linked to an enhancement of the effector abilities of the proliferative progeny subset in HBV inactive carriers (CIBe(−))

After 7-day Ag-specific *in vitro* challenge in presence of IL-2 or IL-15, we tested the expression level of Glut-1, CPT1a and PGC1α in the subset of FSC^{high}/TCF1$^+$ (AP) HBVcore$_{18\text{-}27}$-specific CD8$^+$ cells in CIBe(−). We observed a significant up-regulation of CPT1a and PGC1α and down-regulation of Glut-1 with IL-15 compared to IL-2 treatment (Figure 4A). This IL-15 induced metabolic reprogramming resulted in an increase in the absolute number of cells in the progeny pool, with enhanced degranulation capacity and more intense interferon (IFN)γ and tumor necrosis factor (TNF)α secretion (Figure 4B).

Activated HBV-specific CD8$^+$ progenitor cells in NUC-treated eAg(−) chronic hepatitis B showed a more anabolic profile that was counteracted by IL-15 treatment

On day 7 of specific *in vitro* challenge with HBVcore$_{18\text{-}27}$, we compared Glut-1, CPT1a and PGC1α expression in the AP cell pool between CIBe(−) cases and NUC-treated CHBe(−) patients with detectable cells. FSC^{high} TCF1$^+$ HBV-specific CD8$^+$ cells from NUC-treated CHBe(−) patients showed lower expression of CPT1a and Glut-1 than in CIBe(−) group but a similar level of PGC1α (Figure 5). In NUC treated CHBe(−), IL-15 treatment compared to IL-2 induced an up-regulation of CPT1a and PGC1α expression and a down-regulation of Glut-1 in the HBV-specific CD8$^+$ AP cell pool (Figure 6A). This IL-15 induced metabolic remodeling was associated with an improvement in the effector abilities of the generated progeny. Specifically, we observed with IL-15 treatment an increase in the absolute number of HBV-specific CD8$^+$ cells, an enhanced degranulation capacity and an increase in IFNγ and TNFα secretion (Figure 6B).

Expected highly exhausted HBV-specific CD8$^+$ cell response was restored by the synergistic effect of IL-15 plus anti-PD-L1 in NUC-treated eAg(−) chronic hepatitis B

NUC treatment can restore HBV-specific CD8$^+$ cell response in a subgroup of CHBe(−) patients. There are several clinical predictive variables related to this goal that can be combined to calculate a score that estimates the likelihood of restoration of a functional HBV-multi-specific cytotoxic T cell response during treatment with NUCs,[28] (Figure S1). In a cohort of 48 HLA-A2$^+$ NUC treated CHBe(−) patients (Table S1), we applied this score and observed that those cases with a restoration score >90% had intense-proliferating HBV polymerase(pol)$_{455\text{-}63}$ and HBVcore$_{18\text{-}27}$ specific CD8$^+$ cell responses (>1% HBV-specific CD8$^+$ T cells out of total CD8$^+$ cells) in 88% of cases for both epitopes, whereas this was only found in 43% of HBVpol$_{455\text{-}63}$- and 66% of HBVcore$_{18\text{-}27}$-specific CD8$^+$ cells in cases with intermediate restoration score (16–90%), while in the low score group (0–15%) only 10% of HBVpol$_{455\text{-}63}$- and 32% of HBVcore$_{18\text{-}27}$-specific CD8$^+$ cells had an intense proliferation (Figure 7A). Furthermore, in the ≤15% score group only 5% of patients had HBV-specific CD8$^+$ cells with >1% expansion out of total CD8$^+$ cells against both epitopes while this was observed in 37% of intermediate score cases and 75% of patients with restoration score >90% (Figure 7B). In fact, a linear trend was shown between the number of epitopes with intense responses and the restoration score (Figure 7C).

Based on the previously described data about the IL-15 effect on the metabolic profile in the HBV-specific CD8$^+$ activated progenitor pool, we treated selected HBVcore$_{18\text{-}27}$- or HBVpol$_{455\text{-}63}$-specific CD8$^+$ cell lines from this cohort with different *in vitro* treatments and analyzed the outcomes according to the probability of having a functional response during NUC treatment, calculated by our predictive model,[28] (Figure S1). Data from both epitopes were pooled for statistical analysis. In the restoration score group ≤15%, only 13% of T cell lines expanded with IL-2 and did similarly with IL-2 plus anti-PD-L1 and with a slight improvement with IL-15. However, we obtained the restoration of a reactive response in 75% of cases in the ≤15% restoration score group after treatment with IL-15 plus anti-PD-L1 (Figure 7E). Moreover, IL-15-based treatments not only increased the number of CD8$^+$ cell lines with expansion in this group, but also increased the absolute number of HBV-specific CD8$^+$ cells obtained after expansion per $1{\cdot}10^6$ seeded peripheral blood mononuclear cells (PBMC) (Figures 7E and 7F). To check whether this effect of IL-15 plus anti-PD-L1in the low restoration score group was observed in both HBV-core and HBV-pol specific CD8$^+$ T-cells, we performed a subsequent pilot analysis in a group of cases with restoration score <15%. We tested the proliferation potential after 10-day core$_{18\text{-}27}$ and pol$_{455\text{-}63}$ *in vitro* challenge in presence of IL-2 or IL-15 plus anti-PD-L1. We observed the restoration of proliferation potential with this combination treatment in HBV-core$_{18\text{-}27}$-specific CD8 T-cells but not in HBV-pol$_{455\text{-}63}$-specific cytotoxic T -cells (Figure S2). In the intermediate restoration score group (16–90%), all cultures proliferated with the different treatments, (Figures 7D and 7F) but an increase in the total number of HBV-specific CD8$^+$ cells was also observed with treatments that included IL-15 (Figures 7E and 7F). Finally, CD8$^+$ cell cultures from cases with a high probability of having a functional response proliferated intensely with both IL-2 and IL-15 (Figures 7D–7F).

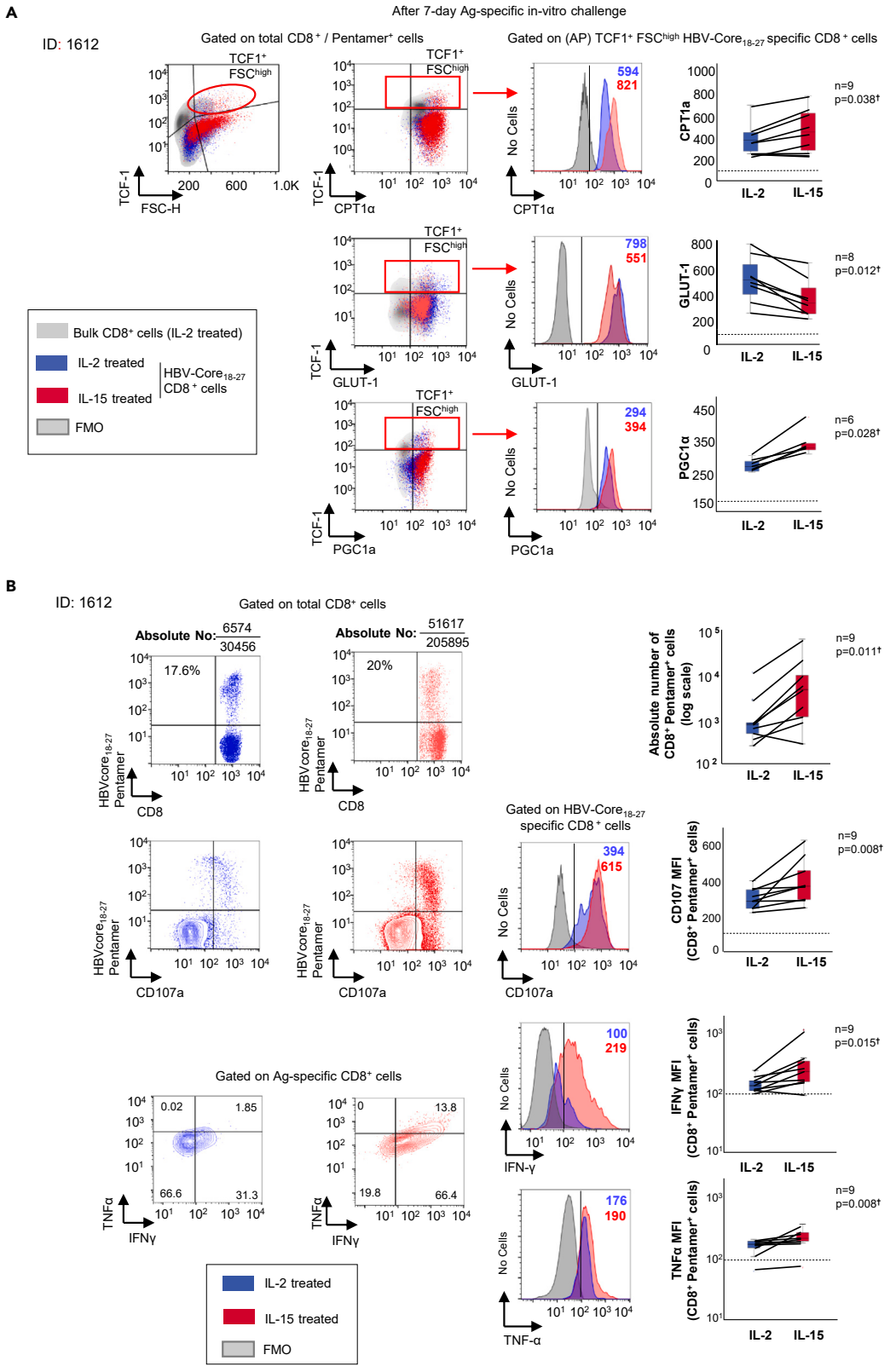
A
After 7-day Ag-specific in-vitro challenge
ID: 1612
Gated on total CD8+ / Pentamer+ cells
Gated on (AP) TCF1+ FSChigh HBV-Core18-27 specific CD8+ cells
TCF1+ FSChigh
TCF-1
FSC-H
CPT1α
GLUT-1
PGC1a
No Cells
594
821
798
551
294
394
CPT1a
GLUT-1
PGC1α
n=9
p=0.038†
n=8
p=0.012†
n=6
p=0.028†
IL-2
IL-15
Bulk CD8+ cells (IL-2 treated)
IL-2 treated
IL-15 treated
FMO
HBV-Core18-27 CD8+ cells
B
ID: 1612
Gated on total CD8+ cells
Absolute No: 6574 / 30456
Absolute No: 51617 / 205895
17.6%
20%
HBVcore18-27 Pentamer
CD8
Absolute number of CD8+ Pentamer+ cells (log scale)
n=9
p=0.011†
Gated on HBV-Core18-27 specific CD8+ cells
CD107a
394
615
CD107 MFI (CD8+ Pentamer+ cells)
n=9
p=0.008†
Gated on Ag-specific CD8+ cells
0.02
1.85
66.6
31.3
0
13.8
19.8
66.4
TNFα
IFNγ
100
219
IFN-γ
IFNγ MFI (CD8+ Pentamer+ cells)
n=9
p=0.015†
176
190
TNF-α
TNFα MFI (CD8+ Pentamer+ cells)
n=9
p=0.008†
IL-2 treated
IL-15 treated
FMO

Figure 4. IL-15 effect on the metabolic profile of activated progenitor HBV-specific CD8$^+$ cells and on the effector abilities of their progeny

(A) Representative BD FACS Calibur dot-plots and histograms and summarizing box-plots depicting the CPT1a, Glut-1 and PGC1α expression on activated progenitor HBVcore$_{18\text{-}27}$ specific CD8$^+$ pool from eAg(−) chronic HBV infection patients (inactive carriers) after 7-day Ag-specific *in vitro* challenge in presence of IL-2 or IL-15. Background gray density plots show the total CD8$^+$ cells as control. In the foreground, IL-2 (blue dots) and IL-15 (red dots) treated HBV-specific CD8$^+$ cells are overlayed.

(B) Representative BD FACS Calibur dot-plots, density-plots and histograms and summarizing box-plots describing the frequency and absolute number of pentamer$^+$/CD8$^+$ cells, CD107 expression and IFNγ and TNFα secretion level on the HBVcore$_{18\text{-}27}$ specific CD8$^+$ effector progeny from eAg(−) chronic HBV infection (inactive carriers) after 7 days Ag-specific *in vitro* challenge in presence of IL-2 or IL-15. The dashed line in the box-plot charts represents the upper-limit of MFI FMO distribution. AP: activated progenitor, FMO: fluorescence minus one, FSC: forward scatter, HBV: hepatitis B virus, IFN: interferon, ID: patient's identification, MFI: mean fluorescence intensity. TNF: tumor necrosis factor. †Wilconxon test. Data are represented as median plus interquartile range.

DISCUSSION

In recent years, different Ag-specific CD8$^+$ progenitor cells have been described during persistent viral infection. Some are located in primary lymphoid organs[2,7,36] but others can be found in the periphery, developing tissue surveillance.[7,35,37] These progenitor cells display a "memory-like" phenotype characterized by PD1 and CD127 expression. As in hepatitis C virus infection,[37] we observed in our study that in both CHBe(−) and CIBe(−) the majority of peripheral HBV-specific CD8$^+$ cells belonged to the memory-like subset, which expressed the memory-linked factor TCF1 and the PD-1$^+$/CD127$^+$ phenotype. We referred to this set as the peripheral QP pool that could be similar to the Ly108$^+$ CD69$^-$ T-exhausted (ex)^{progenitor2} population previously described in a chronic lymphocytic choriomeningitis virus (LCMV) infection model.[7] After Ag encounter, these QP cells underwent a linear differentiation process that was described based on the dynamics of TCF1 expression and FSC level throughout the expansion course by flow cytometry analysis. In the first three days after stimulation, quiescent HBV-specific CD8$^+$ progenitor cells disappeared to transform into the AP pool (TCF1$^+$ FSC^{high}). These cells could develop ACD, as previously suggested by Reiner et al. in a murine model.[5,6] In our work, blocking ICAM-I/LFA1 interaction or decreasing mTORC1 activity by rapamycin treatment reduced the generation of the effector progeny and favored the accumulation of TCF1$^+$ cells. These data suggest a decrease of ACD by blockade of immune synaptosome formation or reduced activation of PI3K pathway. Between day-3 and day-5 after Ag encounter, the AP cell pool began to give rise to the effector progeny subset (TCF1$^-$ FSC^{high}), which would correspond with Ly108$^-$ CD69$^-$ Tex^{intermediate} population in Beltra et al. LCMV model.[7] Finally, after day-7, the PMP pool (TCF1$^-$ FSC^{low}) was observed as the endpoint of the T cell differentiation, which would match with the Tex^{terminal} pool in Beltra's model.[7] In this course, mTORC1 pathway was involved with an intense peak at day-3 in the AP subset and at day-5 in the PP pool under IL-2 culture conditions. It is likely that this strong IL-2-mediated stimulation might not be endured by exhausted HBV-specific CD8$^+$ progenitor cells in NUC-treated CHBe(−) patients, unlike the less activated cells of CIBe(−) subjects. Interestingly, IL-15 modified mTORC1 activity according to P-rpS6 as readout. IL-15 decreased the intensity of the activation peak but extended its duration, resulting in an increase in the number of PP cells and a decrease in the PMP pool. Modulation of mTORC1 activity by IL-15 in the progenitor pool could explain the T cell accumulation and enhanced protection after encounter with TCR cognate-Ag in presence of this cytokine.[38] A previous *in vitro* study to analyze the role of gamma-chain cytokines in Ag-specific CD8$^+$ T cell growth regulation agrees with our data, showing that IL-2 and IL-15 are comparable mitogens upon TCR stimulation, but differ in regulation of protein synthesis because of the different ability to induce PI3K pathway, characterized by temporal and intensity differences in mTORC1 activation.[39] Unequal PI3K signaling during cell division bifurcates sibling fates into progenitor or effector cells with higher activation in the effector progeny.[11] According to our data, this low but more sustained IL-15-induced PI3K activation could be exploited not only to generate memory cells, but also to trigger exhausted progenitor T-cells that do not respond to strong TCR stimulation as occurs in presence of IL-2.

In addition to this effect on PI3K pathway, IL-15 treatment showed an intense effect on the metabolism of activated HBV-specific CD8$^+$ progenitor cells. Previous studies showed that IL-15 was able to induce a catabolic state in chimeric antigen receptor (CAR)-T cells associated with reduced mTORC1 activity and increased CPT1a expression.[25] Moreover, IL-15 can also enhance mitochondrial spare respiratory capacity and mitochondrial biogenesis.[40] T cell fate may be linked to mitochondrial metabolism.[10] Therefore, favoring a catabolic mitochondrial metabolism could promote memory T cell generation. Thus, IL-15 by inducing a catabolic profile could lead to the generation of progenitor cells with better bioenergetic capacity. In our study, IL-15 increased in the AP cell pool the expression of CPT1a, PGC1α and decreased the level of Glut-1. These data suggest a possible increase in FAO and OXPHOS due to increased fatty acid supply, induced by CPT1a up-regulation. Furthermore, these findings imply an increase in mitochondrial mass due to PGC1α-favored biogenesis. Exhausted T-cells have lower levels of PGC1α co-receptor expression than functional cells,[41,42] thus induction of the master regulator of mitochondrial biogenesis could ameliorate the dysfunctional metabolic state of exhausted AP cells. Previous studies show that Glut-1 level and glucose acquisition are decreased in exhausted cells in chronic infection and tumors.[42] Nevertheless, earlier work by Schurich et al., demonstrated a high Glut-1 expression in exhausted effector HBV-specific CD8 cell linked to anabolic metabolism.[43] This observation could suggest that the higher Glut-1 level that we observed in the AP pool similar to PP subset could be due to a higher activation of glycolysis, but this probably only occurs in the effector pool. In fact, it should be clarified that progenitor cells use glucose for fatty acids lipogenesis to fuel mitochondrial metabolism instead of up-taking lipids as occurs in effector cells.[44] Therefore, the high Glut-1 level observed in the AP pool could be related to an activated catabolic state requiring more glucose for fatty acid processing. In any case, the IL-15-induced Glut-1 down-regulation in the AP subset, observed in this study, suggests that both the improved mitochondrial function and decreased activation of PI3K pathway leads to less fueling needs to meet the reduced energy demands with the subsequent reduction in glucose up-take. All these IL-15-induced metabolic changes in the AP pool both at the metabolic level and upon mTORC1 modulation resulted in improved effector capacities of the PP. We must stress

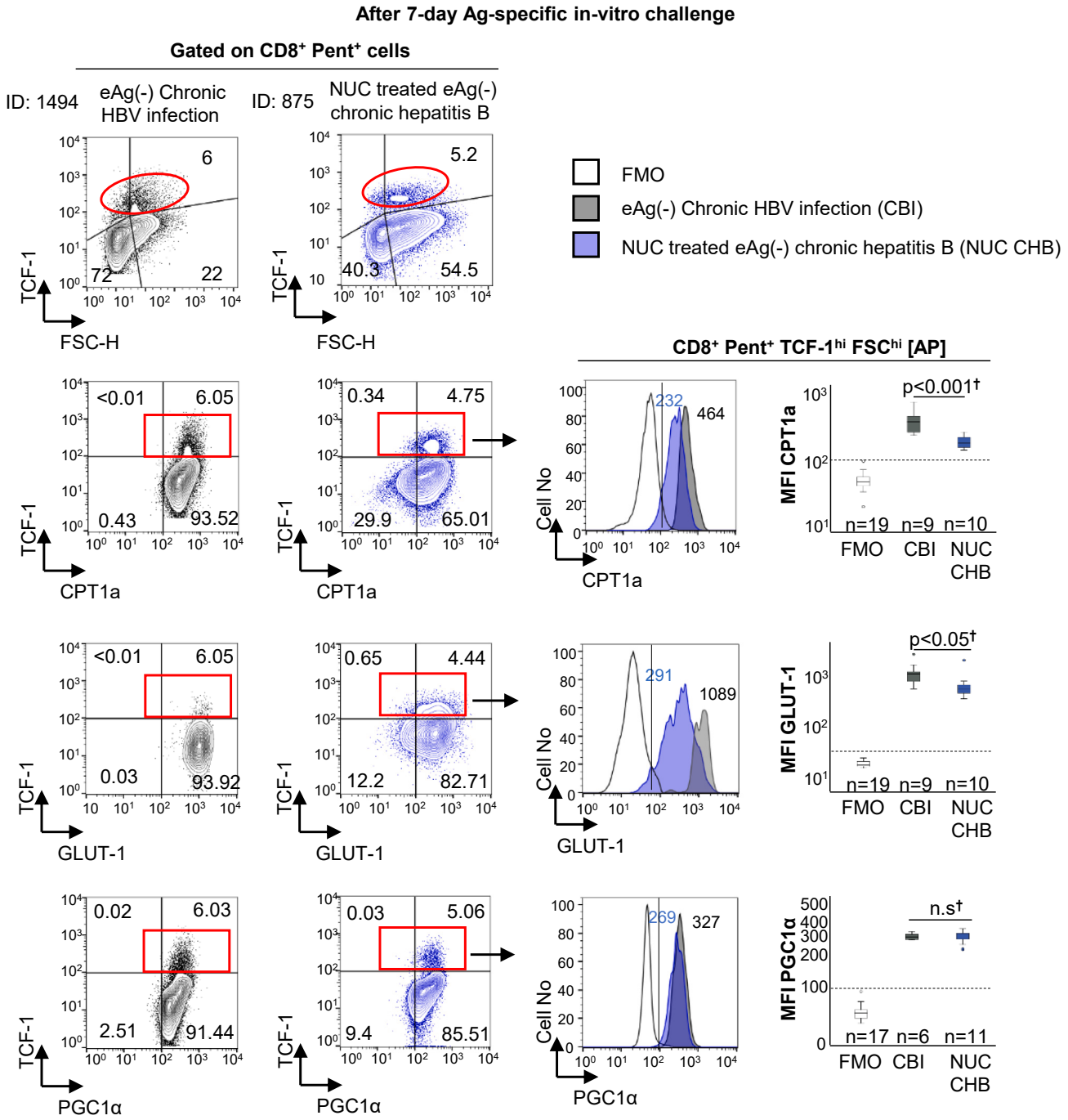

Figure 5. Metabolic profile of activated HBV-specific CD8⁺ progenitor cells according to eAg(−) HBV control

Representative BD FACS Calibur density-plots and histograms and summarizing box-plots depicting the level of CPT1a, Glut-1 and PGC1α expression on $FSC^{high}/TCF1^{+}$ (activated progenitor) $HBVcore_{18\text{-}27}$-specific $CD8^{+}$ cells from eAg(−) chronic HBV infection (inactive carriers) and nucleos(t)ide analogue (NUC)-treated eAg(−) chronic HBV hepatitis after 7-day antigen-specific *in vitro* challenge. The dashed line in the box-plot charts represents the upper-limit of MFI FMO distribution. AP: activated progenitor, CBI: chronic HBV infection, HBV: hepatitis B virus, NUC CHB: NUC-treated chronic hepatitis B, FMO: fluorescence minus one, FSC: forward scatter, ID: patient's identification, MFI: mean fluorescence intensity, NUC: nucleos(t)ide analogue, Pent: pentamer. †Wilconxon test. Data are represented as median plus interquartile range.

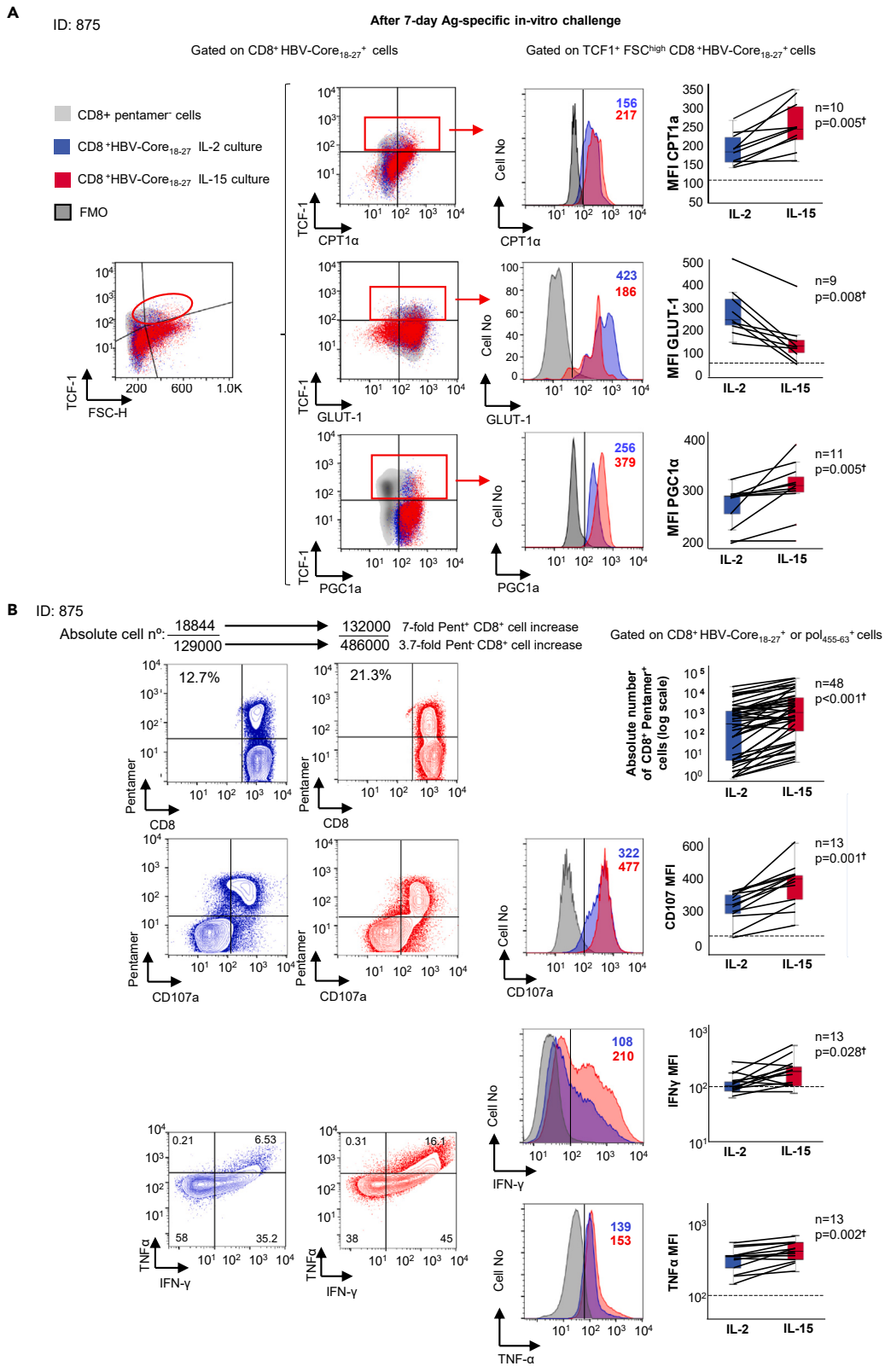
A
ID: 875
After 7-day Ag-specific in-vitro challenge
Gated on CD8+ HBV-Core18-27+ cells
Gated on TCF1+ FSChigh CD8 +HBV-Core18-27+ cells
CD8+ pentamer- cells
CD8 +HBV-Core18-27 IL-2 culture
CD8 +HBV-Core18-27 IL-15 culture
FMO
TCF-1
FSC-H
CPT1α
GLUT-1
PGC1a
Cell No
156
217
423
186
256
379
MFI CPT1a
MFI GLUT-1
MFI PGC1a
n=10
p=0.005†
n=9
p=0.008†
n=11
p=0.005†
IL-2
IL-15
B
ID: 875
Absolute cell nº: 18844 / 129000
132000 7-fold Pent+ CD8+ cell increase
486000 3.7-fold Pent- CD8+ cell increase
Gated on CD8+ HBV-Core18-27+ or pol455-63+ cells
12.7%
21.3%
Pentamer
CD8
CD107a
IFN-γ
TNFα
TNF-α
0.21
6.53
58
35.2
0.31
16.1
38
45
322
477
108
210
139
153
Absolute number of CD8+ Pentamer+ cells (log scale)
CD107 MFI
IFNγ MFI
TNFα MFI
n=48
p<0.001†
n=13
p=0.001†
n=13
p=0.028†
n=13
p=0.002†

Figure 6. Effect of IL-15 on metabolic profile of activated HBV-specific CD8$^+$ progenitor cells and on the effector abilities of their progenies in NUC-treated eAg(−) chronic hepatitis B

(A) Representative BD FACS Calibur dot-plots and histograms and summarizing boxplots depicting the level of CPT1a, Glut-1 and PGC1α expression on FSC^{high}/TCF1$^+$ (activated progenitor) HBVcore$_{18\text{-}27}$-specific CD8$^+$ cells from NUC-treated eAg(−) chronic hepatitis B after 7-day antigen-specific *in vitro* challenge in presence of IL-2 or IL-15. Background gray density plots show the total CD8$^+$ cells as control. In the foreground, IL-2 (blue dots) and IL-15 (red dots) treated HBV-specific CD8$^+$ cells are overlayed.

(B) Representative BD FACS Calibur dot-plots and histograms and summarizing boxplots showing the proliferation ability, CD107 expression and IFNγ/TNFα secretion on total HBV-specific CD8$^+$ cells after 7-day Ag-specific *in vitro* culture in presence of IL-2 or IL-15. The assessment of HBV-specific CD8$^+$ cell effector responses comprised a pool of experiments carried-out for HBVcore$_{18\text{-}27}$- and HBVpol$_{465\text{-}63}$-specific CD8$^+$ cells. FMO: fluorescence minus one, FSC: forward scatter, HBV: hepatitis B virus, IFN: interferon, ID: patient's identification, MFI: mean fluorescence intensity, Pent: pentamer, TNF: tumor necrosis factor. †Wilconxon test. Data are represented as median plus interquartile range.

that all these phenotype and metabolic analysis were performed on HBVcore-specific CD8$^+$ T-cells, so future work should be done to test whether more potentially exhausted T-cells,[45] such as envelope(env)- or pol-specific T-cells, could behave in a different way.

To increase sample size for the study of effector abilities, HBV-core and -pol experiments were pooled. Globally, pol-specific proliferating CD8$^+$ T cell response was less frequently observed than core-specific one under IL-2 condition, probably due to a more severe exhaustion in the pol subset. This finding is in agreement with the recent report stating that the dysregulation of TCF1/Bcl2 expression limits the expansion capacity of pol-specific CD8$^+$ cells in chronic patients.[45]

Based on our previous work, we calculated a probability score for restoration of a multi-specific cytotoxic T cell response in CHBe(−) patients during treatment with NUC. This score is the result of a logistic regression model predicting the probability of having an HBV-multi-specific functional CD8$^+$ T cell response in CHBe(−) patients during NUC treatment as a function of different clinical variables,[28] (Figure S1). We must point out that our predictive model was developed in a Mediterranean cohort and has not been externally validated, so we cannot be sure that our findings can be extended to other CHBe(−) populations. Cases with higher restoration score maintained proliferative cells after Ag-encounter and we were able to analyze in them the expression of different metabolic markers. We observed that in NUC-treated CHBe(−) cases, the expression of Glut-1 and CPT1a in the AP cell subset was significantly lower than in the less exhausted cells of CIBe(−) cases. Interestingly, similar to the effect in CIBe(−) patients, IL-15 *in vitro* treatment was also able to enhance CPT1a and PGC1α expression and decrease Glut-1 level in NUC-treated CHBe(−) cases. This observation encouraged us to pursue an IL-15-based strategy to restore a functional HBV-specific CD8$^+$ T cell response in those CHBe(−) patients with a low HBV-multi-specific cytotoxic T cell response restoration score, according to our previously published predictive model,[28] (Figure S1). Overall, IL-15 treatment alone increased proliferation intensity in cases with a medium-high restoration probability score but was not sufficient for patients with potentially extremely exhausted cells. Nevertheless, in these cases, blockade of the immune check-point PD-1 in combination with IL-15 treatment, but not isolated treatment with anti-PD-L1, restored the expansion capacity of HBV-specific CD8$^+$ cells in 75% of this sort of patients. Unfortunately, the positive effect of combined IL-15/anti-PD-L1 treatment appeared to be limited to HBV core-specific CD8$^+$ T-cells but failed to restore HBVpol-specific CD8$^+$ T cell proliferation in patients with a low restoration probability score, suggesting the involvement of different mechanisms of exhaustion depending on the target epitope. This finding could be related with the downregulation of anti-apoptotic proteins in HBVpol-specific CD8$^+$ progenitor T-cells.[45] Although we did not directly check the PD-1 effect on mitochondrial metabolism, in a murine model of chronic infection, PD-1 was shown to alter glycolytic flux, OXPHOS and decreases PGC1α on exhausted cells, yet anti PD-L1 treatment was able to improve bioenergetic balance.[32] Nevertheless, PD-1 pathway blockade has shown clinical efficacy only in the cases with low level of T cell exhaustion in CHB.[16] Probably, in highly exhausted cells, energy needs after enhancing TCR signaling by blocking PD-1 pathway[15] cannot be supplied by dysfunctional mitochondria. Indeed, PD-1 induction has a supportive effect on TCF-1$^+$ exhausted progenitor cells in the early phase of chronic infection by decreasing TCR signaling in order to sustain the viability of these cells during a persistent infection.[46] In those non-responders to anti-PD-1 treatment, a synergistic effect between IL-15 and PD-1 blockade on mitochondrial metabolism and modulation of T cell activation intensity could be a potential strategy to explore in order to achieve functional cure in CHBe(−),[34] as we suggest in our study.

The effect of PD-1/PD-L1 pathway blockade plus IL-15 treatment on CD8$^+$ T cell effector function has been previously tested in other chronic viral infections[47] and also in tumor-infiltrating CD8$^+$ T-cells unresponsive to PD-1 blockade.[48] In addition, the development of CAR-T cells in an IL-15-rich environment enhances the response to PD-1 blockade in solid tumors.[49] Combined IL-15 blockade with anti-PD-1 or anti-cytotoxic T lymphocyte-associated (CTLA-4) treatments has also yielded promising results in tumor models.[50] In phase-1 human clinical trials, administration of IL-15 in combination with PD-1 blocking antibodies can be safely administrated with promising clinical activity in non-microcytic lung cancer.[51] The findings of these studies correlate with our data and suggest that the combination of IL-15 with PD-1/PD-L1 pathway blockade leads to improved immune response in chronic infections and cancer and could be a potential strategy to achieve functional cure in CHBe(−).[34]

To sum up, our study shows that the restoration of a functional HBV-specific CD8$^+$ T cell response depends on the balance between the intensity of T cell activation and the mitochondrial capacity to supply the energy needs of progenitor cells after Ag encounter. IL-15 induces both an intermediate but sustained mTORC1 activation and a more catabolic profile in the AP cell pool, resulting in an enhanced effector capacity in the PP subset. This effect of IL-15 is especially important in deeply exhausted HBV core-specific CD8$^+$ T-cells, in which restoration of TCR signaling based on PD-1/PD-L1 pathway blockade may likely not be supported by these cells due to cell deficiencies in energy generation. In those NUC-treated CHBe(−) cases with low probability of achieving a functional response during treatment with NUCs, IL-15 combined with anti-PD-L1 treatment restores HBV core-specific CD8$^+$ cell reactivity *in vitro* but could not be effective in HBV pol-specific cells. These strategies should be explored in the future, in combination with standard NUC treatment, to increase the likelihood of obtaining functional cure.[34]

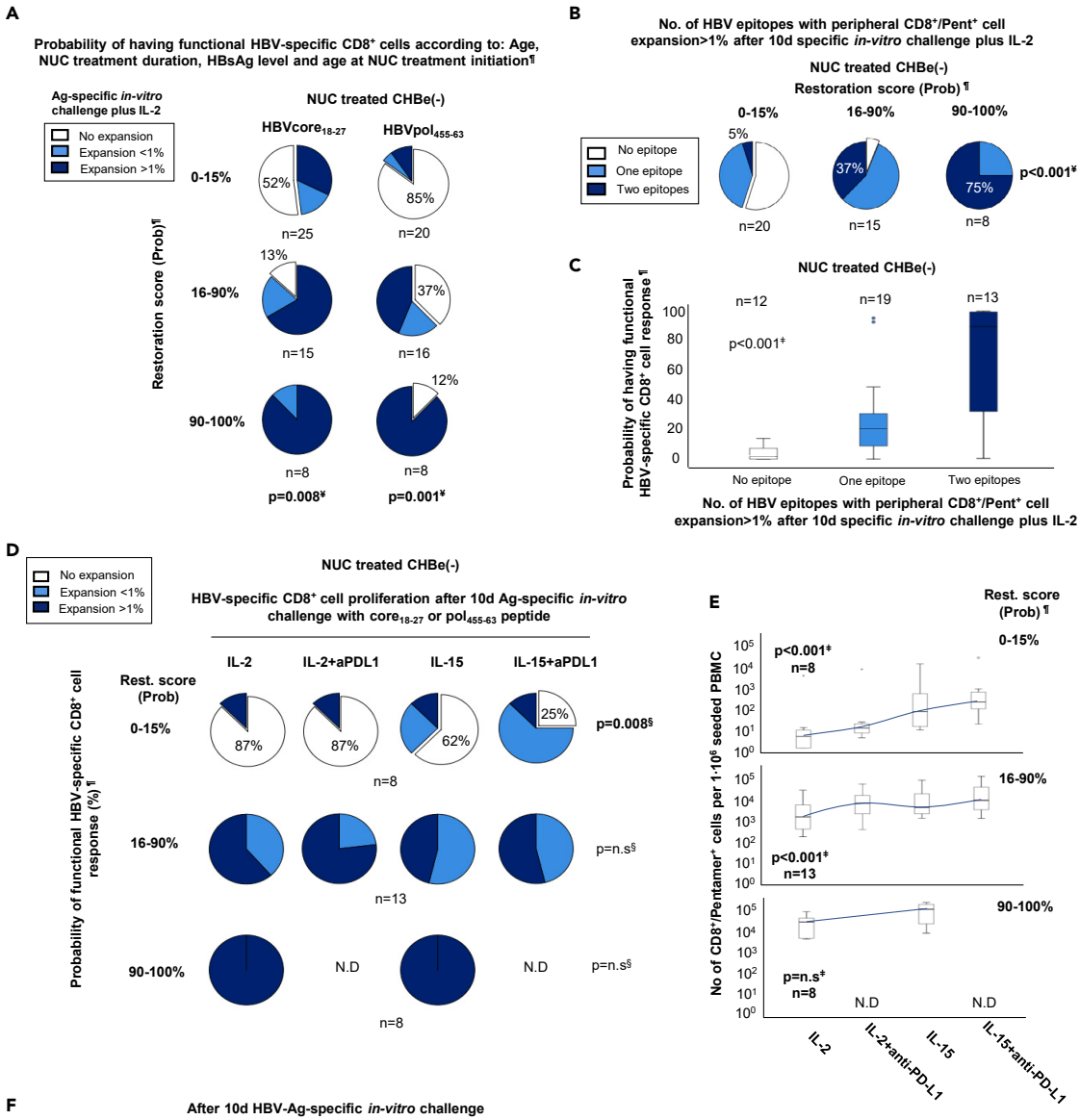

Pat. ID	Prob (%) ¶	Age (decades)	NUC tx dur (years)	Age at tx start (<40 years)	HBsAg log (IU/mL)
600	**3%**	5.4	6.3	No	3.5
467	**25%**	5.3	9.5	No	3.6
387	**>99%**	4.4	10.5	Yes	2.1

Figure 7. *in vitro* restoration of exhausted HBV-specific CD8$^+$ cell response by the synergistic effect of IL-15 plus anti-PD-L1 treatment

In eAg(−) chronic hepatis B patients treated with nucleos(t)ide analogues, (A) Percentage of cases with CD8$^+$ cell proliferation after core$_{18\text{-}27}$- and pol$_{455\text{-}63}$-specific *in vitro* challenge plus IL-2 and, (B) Proportion of cases with proliferation >1% of CD8$^+$ pentamer$^+$ cells out of total CD8$^+$ cells for none, one or two epitopes after IL-2 plus Ag-specific *in vitro* challenge, according to the pre-test probability of having a restored functional HBV-specific CD8$^+$ cell response (restoration score) during NUC treatment.[28]

(C) Positive correlation between the number of epitopes with CD8$^+$ Pentamer$^+$ proliferation >1% after IL-2 plus Ag-specific *in vitro* challenge and the probability of having a functional response during NUC treatment (restoration score).[28]

(D) Percentage of HBV-specific (core$_{18\text{-}27}$ or pol$_{455\text{-}63}$) CD8$^+$ cell lines with Ag-specific expansion after different *in vitro* treatments (IL-2, IL2+anti-PD-L1, IL-15 and IL-15+anti-PD-L1), according to the probability of developing a functional response during treatment (restoration score).[28]

(E) Boxplot charts describing the absolute number of CD8$^+$/Pentamer$^+$ cells per 1x10^6 seeded peripheral blood mononuclear cells after 10days Ag-specific *in vitro* challenge, according to different *in vitro* treatments and the restoration score.[28]

(F) Representative BD FACS Calibur dot-plots showing the expansion ability of HBV-specific CD8$^+$ cells after different *in vitro* treatments together with the values of the predictive variables of the model to define the pre-test probability of having a functional response (restoration score).[28] The figure in the dot-plot shows the percentage of CD8$^+$/Pentamer$^+$ cells out of total CD8$^+$ cells. The figures in the external upper right corner show the total number of CD8$^+$ and CD8$^+$/pentamer$^+$ cells acquired in each experiment. CHBe(−): eAg(−) chronic hepatitis B, dur: duration, HBV: hepatitis B virus, N.D: not done, NUC: nucleos(t)ide analogue, PBMC: peripheral blood mononuclear cells, Prob: probability, Pent: pentamer, pol: polymerase, tx: treatment, Rest: restoration. ¶The calculation of the probability of having a proliferative HBV-specific CD8$^+$ cell response against core and pol (restoration score) during NUC treatment is based on the risk factors: patient age, NUC treatment duration, HBsAg level and age at NUC treatment initiation according to the predictive model defined by Peña-Asensio et al., 2022,[28] (Figure S1). ¥Chi-square test, §Linear trend test, ‡Jonckheere-Terpstra test. Data are represented as median plus interquartile range.

Limitations of the study

The main limitation of the study is that modulation of T cell activation and metabolic phenotype induced by IL-15 treatment was performed only in HBV core-specific CD8$^+$ T-cells and we cannot extrapolate these data directly to other specificities, such as HBV pol or HBV env-specific CD8$^+$ T-cells, which might be more exhausted. Another possible caveat of our work is that we studied HBV-specific cytotoxic T cell response in a Mediterranean cohort, so we cannot be sure that our results can be extended to another non-Caucasian population with a different source of infection and natural history. Finally, in the restoration experiments we used our predictive logistic regression model[28] (Figure S1) to split cases according to the estimated exhaustion level. This model was described by our group recently, but it has not yet been externally validated, therefore this information should be taken with caution.

STAR★METHODS

Detailed methods are provided in the online version of this paper and include the following:

- KEY RESOURCES TABLE
- RESOURCE AVAILABILITY
  - Lead contact
  - Materials availability
  - Data and code availability
- EXPERIMENTAL MODEL AND STUDY PARTICIPANT DETAILS
  - Study design
- METHOD DETAILS
  - Human leukocyte antigen-A2
  - Synthetic peptides and pentamers
  - Antibodies
  - Virological assessment and tissue typing
  - Detection and characterization of the different progenitor and progeny cell pools
  - Ag-specific in-vitro challenge of HBV/CMV-specific CD8$^+$ cells
  - HBV-specific CD8$^+$ cell in-vitro treatments
  - ICAM-I/LFA interaction blockade
- QUANTIFICATION AND STATISTICAL ANALYSIS

SUPPLEMENTAL INFORMATION

Supplemental information can be found online at https://doi.org/10.1016/j.isci.2023.108666.

ACKNOWLEDGMENTS

This study was sponsored by the "Instituto de Salud Carlos III" (ISCIII), Spain, through the "State Plan for Scientific and Technical Research and Innovation 2017–2020", grant PI19/00206 (JRL), co-funded by the European Regional Development Fund (ERDF), E.U., "A way of making Europe".

We are very grateful to the patients for their generous participation in the study and to the Nursing staff from the Endoscopy Unit Guadalajara University Hospital for taking the patients' samples.

AUTHOR CONTRIBUTIONS

Conceptualization: J.-R.L. and J.P.-A. Methodology: J.-R.L. and J.P.-A; Software: J.-R.L.; Formal analysis: J.-R.L., M.T., J.P.-A., and H.C.-S.; Investigation: J.-R.L., J.P.-A., A.G.-P., H.C., E.S.d.V., J.M., and M.T.; Resources: J.-R.L., J.M., E.S.d.V., J.P.-A., and A.G.-P.; Data curation: J.-R.L.; Writing – Original Draft: J.-R.L. and J.P.-A.; Writing – Review and Editing: J.R.L., J.P.-A., M.T., and H.C.-S.; Supervision: J.R.L.; Project Administration: J.R.L.; Funding Acquisition: J.-R.L.

DECLARATION OF INTERESTS

The authors declare that the research was conducted in the absence of any commercial or financial relationships that could be construed as a potential conflict of interest.

INCLUSION AND DIVERSITY

We support inclusive, diverse, and equitable conduct of research.

Received: May 11, 2023
Revised: October 15, 2023
Accepted: December 5, 2023
Published: December 7, 2023

REFERENCES

1. Maini, M.K., Boni, C., Lee, C.K., Larrubia, J.R., Reignat, S., Ogg, G.S., King, A.S., Herberg, J., Gilson, R., Alisa, A., et al. (2000). The role of virus-specific CD8(+) cells in liver damage and viral control during persistent hepatitis B virus infection. J. Exp. Med. *191*, 1269–1280.
2. Paley, M.A., Kroy, D.C., Odorizzi, P.M., Johnnidis, J.B., Dolfi, D.V., Barnett, B.E., Bikoff, E.K., Robertson, E.J., Lauer, G.M., Reiner, S.L., and Wherry, E.J. (2012). Progenitor and terminal subsets of CD8+ T cells cooperate to contain chronic viral infection. Science *338*, 1220–1225.
3. Kratchmarov, R., Magun, A.M., and Reiner, S.L. (2018). TCF1 expression marks self-renewing human CD8(+) T cells. Blood Adv. *2*, 1685–1690.
4. Borsa, M., Barnstorf, I., Baumann, N.S., Pallmer, K., Yermanos, A., Gräbnitz, F., Barandun, N., Hausmann, A., Sandu, I., Barral, Y., and Oxenius, A. (2019). Modulation of asymmetric cell division as a mechanism to boost CD8(+) T cell memory. Sci. Immunol. *4*, eaav1730.
5. Chang, J.T., Palanivel, V.R., Kinjyo, I., Schambach, F., Intlekofer, A.M., Banerjee, A., Longworth, S.A., Vinup, K.E., Mrass, P., Oliaro, J., et al. (2007). Asymmetric T lymphocyte division in the initiation of adaptive immune responses. Science *315*, 1687–1691.
6. Ciocca, M.L., Barnett, B.E., Burkhardt, J.K., Chang, J.T., and Reiner, S.L. (2012). Cutting edge: Asymmetric memory T cell division in response to rechallenge. J. Immunol. *188*, 4145–4148.
7. Beltra, J.C., Manne, S., Abdel-Hakeem, M.S., Kurachi, M., Giles, J.R., Chen, Z., Casella, V., Ngiow, S.F., Khan, O., Huang, Y.J., et al. (2020). Developmental Relationships of Four Exhausted CD8(+) T Cell Subsets Reveals Underlying Transcriptional and Epigenetic Landscape Control Mechanisms. Immunity *52*, 825–841.e8.
8. Lin, W.H.W., Nish, S.A., Yen, B., Chen, Y.H., Adams, W.C., Kratchmarov, R., Rothman, N.J., Bhandoola, A., Xue, H.H., and Reiner, S.L. (2016). CD8(+) T Lymphocyte Self-Renewal during Effector Cell Determination. Cell Rep. *17*, 1773–1782.
9. Adams, W.C., Chen, Y.H., Kratchmarov, R., Yen, B., Nish, S.A., Lin, W.H.W., Rothman, N.J., Luchsinger, L.L., Klein, U., Busslinger, M., et al. (2016). Anabolism-Associated Mitochondrial Stasis Driving Lymphocyte Differentiation over Self-Renewal. Cell Rep. *17*, 3142–3152.
10. Buck, M.D., O'Sullivan, D., Klein Geltink, R.I., Curtis, J.D., Chang, C.H., Sanin, D.E., Qiu, J., Kretz, O., Braas, D., van der Windt, G.J.W., et al. (2016). Mitochondrial Dynamics Controls T Cell Fate through Metabolic Programming. Cell *166*, 63–76.
11. Lin, W.H.W., Adams, W.C., Nish, S.A., Chen, Y.H., Yen, B., Rothman, N.J., Kratchmarov, R., Okada, T., Klein, U., and Reiner, S.L. (2015). Asymmetric PI3K Signaling Driving Developmental and Regenerative Cell Fate Bifurcation. Cell Rep. *13*, 2203–2218.
12. Utzschneider, D.T., Charmoy, M., Chennupati, V., Pousse, L., Ferreira, D.P., Calderon-Copete, S., Danilo, M., Alfei, F., Hofmann, M., Wieland, D., et al. (2016). T Cell Factor 1-Expressing Memory-like CD8(+) T Cells Sustain the Immune Response to Chronic Viral Infections. Immunity *45*, 415–427.
13. Jadhav, R.R., Im, S.J., Hu, B., Hashimoto, M., Li, P., Lin, J.X., Leonard, W.J., Greenleaf, W.J., Ahmed, R., and Goronzy, J.J. (2019). Epigenetic signature of PD-1+ TCF1+ CD8 T cells that act as resource cells during chronic viral infection and respond to PD-1 blockade. Proc. Natl. Acad. Sci. USA *116*, 14113–14118.
14. Siddiqui, I., Schaeuble, K., Chennupati, V., Fuertes Marraco, S.A., Calderon-Copete, S., Pais Ferreira, D., Carmona, S.J., Scarpellino, L., Gfeller, D., Pradervand, S., et al. (2019). Intratumoral Tcf1(+)PD-1(+)CD8(+) T Cells with Stem-like Properties Promote Tumor Control in Response to Vaccination and Checkpoint Blockade Immunotherapy. Immunity *50*, 195–211.e10.
15. Hui, E., Cheung, J., Zhu, J., Su, X., Taylor, M.J., Wallweber, H.A., Sasmal, D.K., Huang, J., Kim, J.M., Mellman, I., and Vale, R.D. (2017). T cell costimulatory receptor CD28 is a primary target for PD-1-mediated inhibition. Science *355*, 1428–1433.
16. Ferrando-Martinez, S., Huang, K., Bennett, A.S., Sterba, P., Yu, L., Suzich, J.A., Janssen, H.L.A., and Robbins, S.H. (2019). HBeAg seroconversion is associated with a more effective PD-L1 blockade during chronic hepatitis B infection. JHEP Rep. *1*, 170–178.
17. Fisicaro, P., Barili, V., Montanini, B., Acerbi, G., Ferracin, M., Guerrieri, F., Salerno, D., Boni, C., Massari, M., Cavallo, M.C., et al. (2017). Targeting mitochondrial dysfunction can restore antiviral activity of exhausted HBV-specific CD8 T cells in chronic hepatitis B. Nat. Med. *23*, 327–336.
18. Berard, M., Brandt, K., Bulfone-Paus, S., and Tough, D.F. (2003). IL-15 promotes the survival of naive and memory phenotype CD8+ T cells. J. Immunol. *170*, 5018–5026.
19. Li, S., Qi, X., Gao, Y., Hao, Y., Cui, L., Ruan, L., and He, W. (2010). IL-15 increases the frequency of effector memory CD8+ T cells in rhesus monkeys immunized with HIV vaccine. Cell. Mol. Immunol. *7*, 491–494.
20. Sandau, M.M., Kohlmeier, J.E., Woodland, D.L., and Jameson, S.C. (2010). IL-15 regulates both quantitative and qualitative features of the memory CD8 T cell pool. J. Immunol. *184*, 35–44.
21. Nolz, J.C., and Richer, M.J. (2020). Control of memory CD8(+) T cell longevity and effector functions by IL-15. Mol. Immunol. *117*, 180–188.
22. Xu, A., Bhanumathy, K.K., Wu, J., Ye, Z., Freywald, A., Leary, S.C., Li, R., and Xiang, J. (2016). IL-15 signaling promotes adoptive effector T-cell survival and memory formation in irradiation-induced lymphopenia. Cell Biosci. *6*, 30.

23. Shourian, M., Beltra, J.C., Bourdin, B., and Decaluwe, H. (2019). Common gamma chain cytokines and CD8 T cells in cancer. Semin. Immunol. *42*, 101307.
24. Felices, M., Lenvik, A.J., McElmurry, R., Chu, S., Hinderlie, P., Bendzick, L., Geller, M.A., Tolar, J., Blazar, B.R., and Miller, J.S. (2018). Continuous treatment with IL-15 exhausts human NK cells via a metabolic defect. JCI Insight *3*, e96219.
25. Alizadeh, D., Wong, R.A., Yang, X., Wang, D., Pecoraro, J.R., Kuo, C.F., Aguilar, B., Qi, Y., Ann, D.K., Starr, R., et al. (2019). IL15 Enhances CAR-T Cell Antitumor Activity by Reducing mTORC1 Activity and Preserving Their Stem Cell Memory Phenotype. Cancer Immunol. Res. *7*, 759–772.
26. Fanning, G.C., Zoulim, F., Hou, J., and Bertoletti, A. (2019). Therapeutic strategies for hepatitis B virus infection: towards a cure. Nat. Rev. Drug Discov. *18*, 827–844.
27. European Association for the Study of the Liver (2017). EASL 2017 Clinical Practice Guidelines on the management of hepatitis B virus infection. J. Hepatol. *67*, 370–398.
28. Peña-Asensio, J., Calvo, H., Miquel, J., Sanz-de-Villalobos, E., González-Praetorius, A., Torralba, M., and Larrubia, J.R. (2022). Model to predict on-treatment restoration of functional HBV-specific CD8(+) cell response foresees off-treatment HBV control in eAg-negative chronic hepatitis B. Aliment. Pharmacol. Ther. *55*, 1545–1559.
29. Menk, A.V., Scharping, N.E., Rivadeneira, D.B., Calderon, M.J., Watson, M.J., Dunstane, D., Watkins, S.C., and Delgoffe, G.M. (2018). 4-1BB costimulation induces T cell mitochondrial function and biogenesis enabling cancer immunotherapeutic responses. J. Exp. Med. *215*, 1091–1100.
30. Choi, B.K., Lee, D.Y., Lee, D.G., Kim, Y.H., Kim, S.H., Oh, H.S., Han, C., and Kwon, B.S. (2017). 4-1BB signaling activates glucose and fatty acid metabolism to enhance CD8(+) T cell proliferation. Cell. Mol. Immunol. *14*, 748–757.
31. Vezys, V., Penaloza-MacMaster, P., Barber, D.L., Ha, S.J., Konieczny, B., Freeman, G.J., Mittler, R.S., and Ahmed, R. (2011). 4-1BB signaling synergizes with programmed death ligand 1 blockade to augment CD8 T cell responses during chronic viral infection. J. Immunol. *187*, 1634–1642.
32. Bengsch, B., Johnson, A.L., Kurachi, M., Odorizzi, P.M., Pauken, K.E., Attanasio, J., Stelekati, E., McLane, L.M., Paley, M.A., Delgoffe, G.M., and Wherry, E.J. (2016). Bioenergetic Insufficiencies Due to Metabolic Alterations Regulated by the Inhibitory Receptor PD-1 Are an Early Driver of CD8(+) T Cell Exhaustion. Immunity *45*, 358–373.
33. Papatheodoridis, G., Vlachogiannakos, I., Cholongitas, E., Wursthorn, K., Thomadakis, C., Touloumi, G., and Petersen, J. (2016). Discontinuation of oral antivirals in chronic hepatitis B: A systematic review. Hepatology *63*, 1481–1492.
34. Calvo Sánchez, H., Peña-Asensio, J., and Larrubia Marfil, J.R. (2022). Current challenges in the functional cure of HBe-Antigen-negative chronic hepatitis B. Rev. Esp. Enferm. Dig. *114*, 441–444.
35. Gerlach, C., Moseman, E.A., Loughhead, S.M., Alvarez, D., Zwijnenburg, A.J., Waanders, L., Garg, R., de la Torre, J.C., and von Andrian, U.H. (2016). The Chemokine Receptor CX3CR1 Defines Three Antigen-Experienced CD8 T Cell Subsets with Distinct Roles in Immune Surveillance and Homeostasis. Immunity *45*, 1270–1284.
36. Im, S.J., Hashimoto, M., Gerner, M.Y., Lee, J., Kissick, H.T., Burger, M.C., Shan, Q., Hale, J.S., Lee, J., Nasti, T.H., et al. (2016). Defining CD8+ T cells that provide the proliferative burst after PD-1 therapy. Nature *537*, 417–421.
37. Wieland, D., Kemming, J., Schuch, A., Emmerich, F., Knolle, P., Neumann-Haefelin, C., Held, W., Zehn, D., Hofmann, M., and Thimme, R. (2017). TCF1(+) hepatitis C virus-specific CD8(+) T cells are maintained after cessation of chronic antigen stimulation. Nat. Commun. *8*, 15050.
38. Richer, M.J., Pewe, L.L., Hancox, L.S., Hartwig, S.M., Varga, S.M., and Harty, J.T. (2015). Inflammatory IL-15 is required for optimal memory T cell responses. J. Clin. Invest. *125*, 3477–3490.
39. Cornish, G.H., Sinclair, L.V., and Cantrell, D.A. (2006). Differential regulation of T-cell growth by IL-2 and IL-15. Blood *108*, 600–608.
40. van der Windt, G.J.W., Everts, B., Chang, C.H., Curtis, J.D., Freitas, T.C., Amiel, E., Pearce, E.J., and Pearce, E.L. (2012). Mitochondrial respiratory capacity is a critical regulator of CD8+ T cell memory development. Immunity *36*, 68–78.
41. Dumauthioz, N., Tschumi, B., Wenes, M., Marti, B., Wang, H., Franco, F., Li, W., Lopez-Mejia, I.C., Fajas, L., Ho, P.C., et al. (2021). Enforced PGC-1alpha expression promotes CD8 T cell fitness, memory formation and antitumor immunity. Cell. Mol. Immunol. *18*, 1761–1771.
42. Reina-Campos, M., Scharping, N.E., and Goldrath, A.W. (2021). CD8(+) T cell metabolism in infection and cancer. Nat. Rev. Immunol. *21*, 718–738.
43. Schurich, A., Pallett, L.J., Jajbhay, D., Wijngaarden, J., Otano, I., Gill, U.S., Hansi, N., Kennedy, P.T., Nastouli, E., Gilson, R., et al. (2016). Distinct Metabolic Requirements of Exhausted and Functional Virus-Specific CD8 T Cells in the Same Host. Cell Rep. *16*, 1243–1252.
44. O'Sullivan, D., van der Windt, G.J.W., Huang, S.C.C., Curtis, J.D., Chang, C.H., Buck, M.D., Qiu, J., Smith, A.M., Lam, W.Y., DiPlato, L.M., et al. (2014). Memory CD8(+) T cells use cell-intrinsic lipolysis to support the metabolic programming necessary for development. Immunity *41*, 75–88.
45. Schuch, A., Salimi Alizei, E., Heim, K., Wieland, D., Kiraithe, M.M., Kemming, J., Llewellyn-Lacey, S., Sogukpinar, Ö., Ni, Y., Urban, S., et al. (2019). Phenotypic and functional differences of HBV core-specific versus HBV polymerase-specific CD8+ T cells in chronically HBV-infected patients with low viral load. Gut *68*, 905–915.
46. Chen, Z., Ji, Z., Ngiow, S.F., Manne, S., Cai, Z., Huang, A.C., Johnson, J., Staupe, R.P., Bengsch, B., Xu, C., et al. (2019). TCF-1-Centered Transcriptional Network Drives an Effector versus Exhausted CD8 T Cell-Fate Decision. Immunity *51*, 840–855.e5.
47. Goshu, B.A., Chen, H., Moussa, M., Cheng, J., and Catalfamo, M. (2020). Combination rhIL-15 and Anti-PD-L1 (Avelumab) Enhances HIVGag-Specific CD8 T-Cell Function. J. Infect. Dis. *222*, 1540–1549.
48. Kim, K.H., Kim, H.K., Kim, H.D., Kim, C.G., Lee, H., Han, J.W., Choi, S.J., Jeong, S., Jeon, M., Kim, H., et al. (2021). PD-1 blockade-unresponsive human tumor-infiltrating CD8(+) T cells are marked by loss of CD28 expression and rescued by IL-15. Cell. Mol. Immunol. *18*, 385–397.
49. Giuffrida, L., Sek, K., Henderson, M.A., House, I.G., Lai, J., Chen, A.X.Y., Todd, K.L., Petley, E.V., Mardiana, S., Todorovski, I., et al. (2020). IL-15 Preconditioning Augments CAR T Cell Responses to Checkpoint Blockade for Improved Treatment of Solid Tumors. Mol. Ther. *28*, 2379–2393.
50. Yu, P., Steel, J.C., Zhang, M., Morris, J.C., and Waldmann, T.A. (2010). Simultaneous blockade of multiple immune system inhibitory checkpoints enhances antitumor activity mediated by interleukin-15 in a murine metastatic colon carcinoma model. Clin. Cancer Res. *16*, 6019–6028.
51. Wrangle, J.M., Velcheti, V., Patel, M.R., Garrett-Mayer, E., Hill, E.G., Ravenel, J.G., Miller, J.S., Farhad, M., Anderton, K., Lindsey, K., et al. (2018). ALT-803, an IL-15 superagonist, in combination with nivolumab in patients with metastatic non-small cell lung cancer: a non-randomised, open-label, phase 1b trial. Lancet Oncol. *19*, 694–704.
52. Larrubia, J.R., Benito-Martínez, S., Miquel, J., Calvino, M., Sanz-de-Villalobos, E., González-Praetorius, A., Albertos, S., García-Garzón, S., Lokhande, M., and Parra-Cid, T. (2011). Bim-mediated apoptosis and PD-1/PD-L1 pathway impair reactivity of PD1(+)/CD127(-) HCV-specific CD8(+) cells targeting the virus in chronic hepatitis C virus infection. Cell. Immunol. *269*, 104–114.

STAR★METHODS

KEY RESOURCES TABLE

REAGENT or RESOURCE	SOURCE	IDENTIFIER
Antibodies		
anti-human CD3 mAb (Alexa Fluor® 647 conjugate)	BioLegend	Cat # 300416, RRID:AB_389332, Clone UCHT1
anti-human CD8 mAb (PerCP conjugate)	BioLegend	Cat # 344708, RRID:AB_1967149, Clone SK1
anti-human CD8 amAb (PE-Cyanine7 conjugate)	eBioscience	Cat # 25-0088-42, RRID:AB_1659702, Clone RPA-T8
anti-human TCF1/TCF7 mAb (Alexa Fluor® 647 conjugate)	Cell Signaling Technology	Cat # 6709 RRID:AB_2797631, Clone C63D9
anti-human CX3CR1 mAb (FITC)	BioLegend	Cat # 341605, RRID:AB_1626276, Clone 2A9-1
anti-human CD279 (PD-1) mAb (FITC)	BD Pharmingen	Cat # 557860, RRID:AB_2159176, Clone MIH4
anti-human CD127 (IL-7Rα) mAb (Alexa Fluor® 647)	BioLegend	Cat # 351318, RRID:AB_10896063, Clone A019D5
anti-human Glut1 mAb (Alexa Fluor® 488-conjugate)	R&D Systems	Cat # FAB1418G, RRID:AB_2941076, Clone 202915
anti-human PGC1α mAb (Alexa Fluor® 488-conjugate)	Santa Cruz Biotechnology	Cat # sc-518025, RRID:AB_2890187, Clone D-5
Anti-human CPT1A mAb (Alexa Fluor® 488)	Abcam	Cat # ab171449, RRID:AB_2714024, Clone 8F6AE9
Anti-Human Phospho-S6 Ribosomal Protein (Ser235/236) XP® Rabbit mAb (Alexa Fluor® 488 Conjugate)	Cell Signaling Technology	Cat # 4803, RRID:AB_916158, Clone D57.2.2E
anti-human CD107a (LAMP-1) mAb (Alexa Fluor® 488-conjugate)	BioLegend	Cat # 328610, RRID:AB_1227504, Clone H4A3
anti-human INF-alpha mAb (FITC conjugate)	R&D Systems	Cat# IC285F, RRID:AB_357308, Clone 25723
anti-human TNF-α mAb (Alexa Fluor® 647 conjugate)	BioLegend	Cat # 502916, RRID:AB_493123, Clone MAb11
anti-human HLA-A2 mAb (FITC conjugate)	BioLegend	Cat # 343304, RRID: AB_1659245, Clone BB7.2
Chemicals, peptides, and recombinant proteins		
Ficoll-Hypaque TM PLUS	Cytiva	Cat # 17144002
Roswell Park Memorial Institute medium (RPMI) 1640 1x with L-Glutamine	Corning	Cat # 10'040CV
Dimethyl sulfoxide (DMSO)	Sigma-Aldrich	Cat # 276855
Heat-Inactivated Fetal Bovine serum (HI FBS)	Gibco	Cat # 10082-147
CTS Optimizer T cell expansion SFM	Thermo Fisher Scientific	A1048501
Antibiotic-Antimycotic	Gibco	Cat # 15240-062
L-Glutamine	Gibco	Cat # 25030-032
autoMACS® Running Buffer – MACS® Separation Buffer	Miltenyi Biotec	Cat # 130-091-221
Brefeldin A	Sigma-Aldrich	Cat #B6542
Recombinant Human IL-2 Protein	R&D Systems	Cat # 202-IL
Recombinant Human IL-15 Protein	R&D Systems	Cat # 247-IL
BD FACS Flow Sheat Fluid	BD Pharmigen	Cat # 342003
HBV core antigen 18-27 lyophilized peptide	Proimmune	Cat # P023-0A
HBV Pol 455-463 lyophilized peptide	Proimmune	Cat # P778-0A
HCMV pp65 495-504 lyophilized peptide	Proimmune	Cat # P008-0A
Critical commercial assays		
Pro5® MHC Class I Pentamer HBV core antigen 18-27 (PE conjungate)	Proimmune	Cat # F023-2A, Allele A*02:01, peptide code:23, Peptide sequence: FLPSDFFPSV
Pro5® MHC Class I Pentamer HBV Pol 455-463 (PE conjungate)	Proimmune	Cat # F778-2A, Allele A*02:01, peptide code:778, Peptide sequence: GLSRYVARL
Pro5® MHC Class I Pentamer HCMV pp65 495-504 (PE conjungate)	Proimmune	Cat # F008-2A, Allele A*02:01, peptide code:8, Peptide sequence: NLVPMVATV

(*Continued on next page*)

Continued

REAGENT or RESOURCE	SOURCE	IDENTIFIER
Cytofix/Cytoperm™ Fixation/Permeabilization Solution Kit	BD Pharmigen	Cat # 554714
Human FoxP3 buffer set	BD Pharmigen	Cat # 560098
Anti-PE Microbeads	Miltenyi Biotec	Cat # 130-048-801
Software and algorithms		
FlowJo™ software v10.7.1	Becton Dickinson Bioscience	Cat # Non-applicable
IBM© SPSS© 25 Statistics software	IBM Corporation	Cat # Non-applicable

RESOURCE AVAILABILITY

Lead contact

Subsequent inquiries and requests for materials and chemicals should be sent to and will be fulfilled by the lead contact, Dr. Juan-Ramón Larrubia (juan.larrubia@uah.es).

Materials availability

This study did not generate new unique reagents to be shared.

Data and code availability

- On request, the lead contact will share the original data reported in this article.
- This article contains no original code.
- Any extra data necessary to reanalyze the data given in this research is accessible upon request from the lead contact.

EXPERIMENTAL MODEL AND STUDY PARTICIPANT DETAILS

Study design

We carried-out an analytical cross-sectional study. We enrolled 22 CIBe(-) [control group] and 44 NUC-treated CHBe(-) HLA-A2$^+$ patients from Guadalajara University Hospital Viral Hepatitis Clinic, (Table S1). Clinical diagnosis and treatment indication were performed according to the European Association for the Study of the Liver (EASL) guidelines.[27] In all cases at recruitment, a serum and a blood sample were taken to quantify hepatitis B surface (HBs)Ag (logIU/mL), HBV DNA (logIU/mL), and alanine aminotransferase (ALT) (IU/mL) levels and for the immunological tests. PBMC were obtained by Fycoll-Paque (Cytiva, Sweeden) gradient and cryopreserved up to the study. Age, sex at birth and ethnic origin were also recorded and were similarly distributed among the groups compared (Table S1). Sex at birth was recorded from the patient's own information. Patients were recruited consecutively from the Viral Hepatitis Clinic database, regardless of sex at birth or self-reported gender. Gender was not registered in this study. Study patients were middle-aged adults with a median age of 48 years (IQR: 14) in the NUC-treated CHBe(-) group and 49 year (IQR: 20) in the CIBe(-) group (Table S1). The duration of NUC treatment (years) and the age at treatment start (years) were also recorded in NUC-treated CHBe(-) cases. At treatment start for NUC-treated CHBe(-) and at the first appointment for CIBe(-), HBV DNA (logIU/mL), ALT (IU/mL), and liver fibrosis, estimated by transient liver elastography with FibroScan-402® (Echosens, France), were retrospectively obtained. We excluded patients co-infected with hepatitis C, hepatitis D, human immunodeficiency virus or cirrhosis.

Directly ex-vivo analysis of Ag-specific CD8$^+$ cell memory-like and TCF1 phenotypes were carried out to describe the peripheral QP cells. From peripheral QP cells of CIBe(-) patients, we tracked the generation of AP, PP, and PMP cells after HBV-specific in-vitro challenge in presence of IL-2. These cell subsets were discriminated through TCF1 and FSC level by flow-cytometry. In these experiments, CD8$^+$ cell response against CMV was used as internal control. This Ag-specific in-vitro differentiation would mimic the ex-vivo linear differentiation proposed by Beltra et al. in a mice model of LCMV chronic infection.[7] In these T-cell pools sequentially developed after Ag-encounter, we analyzed the following immunological features: memory-like phenotype, metabolic profile, mTORC1 activation, and effector abilities. We compared this IL-2-mediated differentiation process with that observed after Ag-encounter in presence of IL-15. In all NUC-treated CHBe(-) patients, we perform the same Ag-specific proliferation assay to test the expansion ability and effector capacities of the effector progeny pool and metabolic profile of the AP subset in presence of IL-2, and were compared with those observed in CIBe(-). In NUC-treated CHBe(-), we also tested the potential IL-15 role to repair effector function of PP and metabolic profile of AP subsets. The likelihood of restoration of functional HBV-multi-specific cytotoxic T-cell response during NUC treatment (restoration score) was calculated in NUC-treated CHBe(-), based on patient age (decades), HBsAg (logIU/mL) level, NUC therapy starting-point (before or after 40-year age) and treatment duration (years), according to a previously published logistic regression predictive model,[28] (Figure S1). We analyzed the role of IL-15+/-anti-PD-L1 to restore HBV-specific CD8$^+$ cell reactivity in NUC-treated CHBe(-), according to this restoration score as a subrogate of the level of baseline T-cell

exhaustion. The Research Ethical Committee of the Guadalajara University Hospital (Spain) approved the study protocol, which was conformed to the ethical guidelines of the 1975 Declaration of Helsinki. All the patients enrolled in the study gave written informed consent and all the experiments conformed to regulatory standards.

METHOD DETAILS

Human leukocyte antigen-A2

Screening for HLA-A2 haplotype was performed by staining with anti-HLA-A2 fluorescein 5-isothiocyanate (FITC) monoclonal antibody (mAb), (Clone BB7.2), (Biolegend, San Diego, CA).

Synthetic peptides and pentamers

HLA-A2-restricted peptides corresponding to the genotype D HBVcore$_{18\text{-}27}$, HBVpol$_{455\text{-}63}$ and CMVpp65$_{495\text{-}504}$, and phycoerytrin-(PE)-conjugated HLA-A2/peptide pentameric complexes (pentamer) loaded with the same HBV and CMV peptides were purchased from ProImmune (Oxford, UK).

Antibodies

The following mouse anti-human monoclonal antibodies (mAb) were used for flow cytometry: anti-CD3-Alexa Fluor (AF) 647, (Biolegend, San Diego, CA, clone UCHT1), anti-CD8-peridinin chlorophyll(PerCP), (Biolegend, San Diego, CA, clone SK1), anti-CD8-phycoerytrin-(PE)-cyanine(Cy)7,(eBioscience Inc, San Diego, CA, clone rpa-t8), anti-TCF-1-AF 647, (Cell Signaling, Boston, MA, clone 7FIA10), anti-CX3CR1-FITC, (Biolegend, San Diego, CA, clone 2A9-1), anti-PD-1-FITC, (Becton Dickinson Bioscience, San Jose, CA, clone MIH4), anti-CD127-AF 647, (Biolegend, San Diego, CA, clone, A019D5), anti-Glut1-AF488, (R&D Systems, Minneapolis, MN, clone 202915), anti-PGC1α-AF488, (Santa Cruz Biotechnology, Santa Cruz, CA, Clone D-5), anti-CPT1a-AF488 (Abcam, UK, clone 8F6AE9), anti-P-rpS6-AF488 (Cell Signaling, Boston, MA, clone D57.2.2E), anti-CD107a-AF488, (Biolegend, San Diego, CA, clone H4A3), anti-IFNγ FITC, (R&D Systems, Minneapolis, MN, clone RMMA-1), anti-TNFα AF647 (Biolegend, San Diego, CA, clone MAb11).

Virological assessment and tissue typing

HBeAg and anti-HBeAg were tested by chemiluminescent microparticle immunoassay (Abbott, IL). HBsAg was quantified by Elecsys® HBsAg II quant II (Roche Diagnostics, Switzerland). HBV DNA was measured by COBAS® AmpliPrep/COBAS® TaqMan® HBV Test, v2.0 (Roche Diagnostics, Switzerland).

Detection and characterization of the different progenitor and progeny cell pools

To detect HBV-specific CD8$^+$ cells, 1x10^6 PBMC were stained for 10 min at room temperature at saturating concentration of PE-labelled pentamers in Roswell Park Memorial Institute (RPMI) 1640 medium plus 10% heat inactivated fetal bovine serum (HI-FBS), (Thermo Fisher Scientific, MA). Cells were washed in phosphate buffered saline and then incubated at 4°C for 20 min with saturating concentrations of directly conjugated anti-CD8-PerCP mAb. Subsequently after washing, cells were stained with the different markers as described below.

In NUC treated CHBe(-) and CIBe(-), to visualize the different progenitor and progeny subsets in the heterogenous peripheral HBV-specific CD8$^+$ pool, we tracked the differentiation process of CD8$^+$ T-cells after Ag-specific in-vitro challenge by TCF-1 expression level and the FSC value. The FSC^{low} pool comprised the QP pool (TCF1$^+$) and the PMP subset (TCF1$^-$). The FSC^{high} population encompassed the AP pool (TCF1$^+$) and the PP subset (TCF1$^-$). These four populations generated *in vitro* would mimic the linear differentiation process of exhausted Ag-specific CD8$^+$ T -cells proposed by Beltra et al.[7] from peripheral Tex^{progenitor2} pool ≈ QP, which after activation (AP) would give rise to Tex^{intermediate} cells ≈ PP, and finally to Tex^{terminal} subset ≈ PMP.

Directly ex-vivo, PD-1, CD127, CX3CR1 and TCF-1 phenotypes were assessed in the QP subset of HBV and CMV-specific CD8$^+$ cells. In HBV patients, PE-pentamer$^+$ cells were enriched by miniMACS magnetic beads (Milteny Biotec, Germany) following manufacturer's protocol to obtain enough CD8$^+$/Pentamer$^+$ cells to test ex-vivo QP cell phenotypes.

To simulate in-vitro the differentiation process of the QP subset after Ag encounter, in a group of CIBe(-) co-infected with CMV, the dynamics of the different subsets of HBV- and CMV-specific CD8$^+$ cells and the level of P-rpS6 in presence of IL-2 or IL15 were monitored at baseline, day-3, day-5 and day-7 after Ag-specific in-vitro challenge. As negative control of mTORC1 activation was used rapamycin at 100 ηM (Sigma-Aldrich Inc, St. Louis, MO). In CIBe(-) and NUC-treated CHBe(-), Glut-1, PGC1α, CPT1a, PD-1 and CD127 phenotypes were assessed after Ag-specific stimulation at day-7 in AP subset, because at that moment AP cells have already completed their initial three divisions[8] with IL-2 and IL-15. CD107a expression and IFNγ and TNFα secretion were tested at day-10 in the progeny, which is the day with relative highest expansion both with IL-2 and IL-15.

For surface staining, PBMC were first labelled with pentamers and CD8 mAb as previously described. After washing, PBMCs were stained for 30 min at room temperature with anti-CD127-AF647, anti-PD-1-FITC, anti-CX3CR1-FITC or anti-Glut1-AF488. For degranulation assay and IFNγ and TNFα staining, PBMC were Ag-specific in-vitro challenged for 5h at 37°C at 1x10^6 cells/mL in RPMI 1640, plus 10% HI-FCS, in the presence of Brefeldin A (10 μg/mL; Sigma-Aldrich Inc, St. Louis, MO), during the last 4h. Cells were washed, and surface stained with PE-pentamers as above. After a further wash, cells were subjected to intracellular staining using Cytofix-Cytoperm (BD Bioscience, San Jose, CA) to

permeabilize and fix cells, followed by staining with anti-IFNγ-FITC or anti-TNFα-AF647 mAb. For degranulation test, anti-CD107a-AF488 was added at the beginning of the stimulation.

For the TCF-1, P-rpS6, PGC1α and CPT1a intracellular staining, after anti-CD8 and pentamer staining, PMBCs were fixed and permeabilized using Human FoxP3 Buffer Set (BD Bioscience, San Jose, CA), according to manufacturer's protocol. After subsequent washing, PBMCs were stained with anti-TCF-1-AF647, anti-PGC1α-AF488, anti-P-rpS6-AF488 or anti-CPT1a-AF488 for 30 min at room temperature.

In all cases, after a final washing, stained cells were acquired on a Becton Dickinson FACS® Calibur flow-cytometer. Percentage of positive cells and mean fluorescence intensity (MFI) was recorded. Fluorescence minus one (FMO) was used as negative control. All the experiments were analyzed on FlowJo™ software v10.7.1 (Becton Dickinson Bioscience, San Jose, CA).

Ag-specific in-vitro challenge of HBV/CMV-specific CD8$^+$ cells

PBMC were resuspended at a concentration of 1x10^6/mL in complete T-cell medium plus 10% HI-FBS (Thermo Fisher Scientific, MA). Cells were stimulated with 1uM of one of the different HBV/CMV peptides, in a 96-well plate, as previously described.[1,52] Recombinant IL-2 or IL-15 was added on day 2 and 5 of culture (R&D Systems, MN) based on a previous pilot study to test the effect of single or repeated cytokine administration on metabolic markers and proliferation (Figure S3). Final cytokine concentrations were 25 IU/mL for IL2 and 10ηg/mL for IL-15 as previously published.[25] Cells were analyzed after 7 and 10 days of Ag-specific in-vitro challenge to test the metabolic profile of AP and the function of effector cells respectively.

HBV-specific CD8$^+$ cell in-vitro treatments

PBMC were seeded in 96 well plates at a concentration of 1x10^6 cell/mL in complete T-cell medium plus 10% HI-FBS. Cells were stimulated with HBVcore$_{18\text{-}27}$ or HBVpol$_{455\text{-}63}$ for ten days in presence of IL-2 (25 IU/mL) or IL-15 (10ηg/Ml) or IL-2 plus anti-PD-L1 (10 μg/mL), (eBioscience, San Diego, CA) or IL-15 plus anti-PD-L1. Anti-PD-L1 mAbs were added 2h before the stimulation with the specific peptide. IL-2 and IL-15 were administered 48 and 96h post Ag-stimulation. The intensity of proliferation was tested at day-10 as the percentage of CD8$^+$/Pentamer$^+$ cells out of total CD8$^+$ cells. The diverse treatments were assessed in representative NUC-treated CHBe(-) patients with different degree of restoration score according to the logistic regression equation showed in Figure S1, recently published by our group[28]

ICAM-I/LFA interaction blockade

In order to test the involvement of ACD in the AP pool differentiation, the interaction between ICAM-I and LFA-1 was assessed. Blocking anti-ICAM-I mAb (Thermo Fisher Scientific, MA, clone HA58) was added to the cell culture at 10μg/mL for 30 min before adding the specific peptides. The cultures were carried out in presence of IL-2 or IL-15. Cultures without anti-ICAM-I were performed as controls. After 5-day Ag-specific in-vitro challenge, PBMC were collected and the percentage of TCF1$^+$/FSC^{high} CD8$^+$ Pentamer$^+$ cells was assessed.

QUANTIFICATION AND STATISTICAL ANALYSIS

Quantitative and categorical variables are summarized as median plus IQR and as frequency distribution respectively. Chi-square, Mann-Whitney-U, Wilcoxon, Friedman, linear trend, and Jonckheere-Terpstra tests were employed where appropriate. Data were analyzed with IBM© SPSS© 25 Statistics software. All the tests were two tailed and with a $p<0.05$ significance level. The statistical details of expermients can be found in figure, figure legends and results.